Fuel 396 (2025) 135290

Contents lists available at ScienceDirect

Fuel

journal homepage: www.elsevier.com/locate/jfue

Power- and biomass-to-liquid processes with fuel-assisted solid oxide electrolysis cells and water gas shift-adjusted systems: A techno-economic analysis

Samuel M. Krämer[a], Anders S. Nielsen[b,c], Simon Maier[d], Simone Mucci[a,e], Magne Hillestad[f], Odne S. Burheim[c,*]

[a] Process Systems Engineering (AVT.SVT), RWTH Aachen University, Aachen, 52074, Germany
[b] Department of Engineering Science, University of Oxford, Parks Road, Oxford, OX1 3PJ, United Kingdom
[c] Department of Energy and Process Engineering, Norwegian University of Science and Technology, Trondheim, 7491, Norway
[d] German Aerospace Center (DLR), Pfaffenwaldring 38-40, Stuttgart, 70569, Germany
[e] Department of Chemical Engineering, KU Leuven, Leuven, 3001, Belgium
[f] Department of Chemical Engineering, Norwegian University of Science and Technology, Trondheim, 7491, Norway

HIGHLIGHTS

- Develops novel process variants of the power- and biomass-to-liquid fuel process.
- Integrates fuel-assisted solid oxide electrolysis cells to reduce energy demands.
- Exploits water gas shift-adjusted system to adapt to varying electricity prices.
- Net production costs for sustainable aviation fuels are between 2.66 and 3.22 €/kg.

ARTICLE INFO

Keywords:
Power- and biomass-to-liquid process
Fuel-assisted solid oxide electrolysis
Water gas shift adjusted system
Techno-economic analysis
Fischer–Tropsch synthesis
Sustainable aviation fuels (SAF)

ABSTRACT

In the pursuit of mitigating climate change, sustainable aviation fuels (SAFs) present a promising solution for defossilizing long-haul air travel. Power- and biomass-to-liquid (PBtL) processes, which combine renewable hydrogen and non-crop-based biomass *via* Fischer–Tropsch (FT) synthesis, offer a pathway to SAF production. However, the high electricity demand for hydrogen production *via* electrolysis poses a significant economic challenge. Therefore, this study investigates the integration of fuel-assisted solid oxide electrolysis cells (FASOECs) and adjustments to the water gas shift (WGS) equilibrium in PBtL processes, to reduce the electricity demand for hydrogen production and adapt to potentially fluctuating electricity prices. The results indicate that WGS adjustments reduce specific electric energy demands but compromise carbon efficiency and fuel production rates. Conversely, FASOEC-based process configurations exhibit higher energy efficiencies when the FT tail gas purge stream is utilized in the FASOEC anode. Furthermore, all considered configurations are thermally self-sufficient when heat integration is performed. A techno-economic analysis using TEPET for Norway in 2023 reveals that the WGS-adjusted configurations consistently outperform FASOEC process variants in terms of net production costs (NPC). Among the evaluated configurations, the WGS-adjusted processes demonstrate the greatest economic competitiveness, with NPC values as low as 2.66 $€_{2023}/kg_{fuel}$ (1.94 $€_{2023}/l_{fuel}$), while the fuel-assisted PBtL recycle case generates the least economically competitive process variant with an NPC value of 3.22 $€_{2023}/kg_{fuel}$ (2.35 $€_{2023}/l_{fuel}$). Additionally, the FT tail gas purge stream emerges as a valuable resource for reducing specific electrolysis energy demands in the Purge-to-Fuel configuration, yielding a reduced NPC value of 3.00 $€_{2023}/kg_{fuel}$ (2.19 $€_{2023}/l_{fuel}$) while retaining the same carbon efficiency as the conventional PBtL process (3.12 $€_{2023}/kg_{fuel}$ (2.27 $€_{2023}/l_{fuel}$)). Key cost drivers include electricity, SOEC stack replacement, and biomass, with the Acid gas cleaning unit identified as a major source of carbon losses (~75 %). This study highlights critical trade-offs between energy and carbon efficiency, emphasizing the need for optimized purge stream utilization and WGS equilibrium adjustments to enhance the commercial viability of SAF production.

* Corresponding author.
Email addresses: samuel.kraemer@rwth-aachen.de (S.M. Krämer), anders.nielsen@eng.ox.ac.uk (A.S. Nielsen), simon.maier@dlr.de (S. Maier), simone.mucci@avt.rwth-aachen.de (S. Mucci), magne.hillestad@ntnu.no (M. Hillestad), burheim@ntnu.no (O.S. Burheim).

https://doi.org/10.1016/j.fuel.2025.135290
Received 29 January 2025; Received in revised form 24 March 2025; Accepted 2 April 2025

Nomenclature

Acronyms

ACC	Annualized capital costs
AGC	Acid gas cleaning
ASF	Anderson–Shulz–Flory distribution
BtL	Biomass-to-liquid
CAPEX	Capital investment expenditure
EC	Equipment costs
EFG	Entrained flow gasifier
FAPBtL	Fuel-assisted power- and biomass-to-liquid
FASOEC	Fuel-assisted solid oxide electrolysis cell
FCI	Fixed capital investment
FT	Fischer–Tropsch
GHGE	Greenhouse gas emissions
HHV	Higher heating value
LHV	Lower heating value
NPC	Net production cost
OPEX	Operational expenditure
PBtL	Power- and biomass-to-liquid
PEM	Polymer electrolyte membrane
PtL	Power-to-liquid
Purge-tF	Purge-to-fuel
RWGS	Reverse water gas shift
SAF	Sustainable aviation fuel
SOEC	Solid oxide electrolysis cell
WGS	Water gas shift
WGS-adj	Water gas shift-adjusted PBtL

1. Introduction

The global climate crisis, driven by anthropogenic greenhouse gas emissions (GHGE), represents an unprecedented challenge to human civilization. Addressing this crisis requires a comprehensive array of measures that span all sectors of society. Notably, the transport sector stands as a significant contributor, emitting 8.9 $GtCO_{2,eq}$ of greenhouse gases annually, constituting 15 % of global emissions and increasing at a rate of 1.8 % per year [1]. Despite the potential for electrification in many transport modes, long-haul aviation, which generates 7 % of all transport emissions, appears impractical due to the low energy densities of batteries and hydrogen fuel cells [2]. Instead, high energy density fuels, such as renewably produced kerosene-like jet fuel, offer promising alternatives to conventional fossil fuels in this sector [3].

The pursuit of sustainable alternatives to fossil fuels in aviation has led to a growing interest in liquid fuels produced *via* Fischer–Tropsch (FT) synthesis [4,5]. Power-to-liquid processes (PtL) that utilize CO_2 from sustainable sources (*e.g.*, unavoidable point sources and direct air carbon capture units [6]) require costly electrical energy as the sole energy source. In contrast, biomass-to-liquid (BtL) and power- and biomass-to-liquid (PBtL) processes with water gas shift (WGS) reactors utilize biomass as a source of both carbon and energy, thereby eliminating the need for an additional carbon source while reducing the electricity requirements. Through gasification, biomass is converted into syngas (a mixture of mainly H_2 and CO), which undergoes FT synthesis to produce biofuels. Moreover, the integration of renewable energy sources, such as solar and wind power for electrolytic hydrogen production, enhances the sustainability of PBtL processes. This strategic addition of hydrogen adjusts the syngas H_2/CO ratio, thus reducing carbon losses and increasing fuel yield [3,5,7].

Advantages of FT-based BtL and PBtL processes include the use of a mature fuel synthesis technology (*i.e.*, FT reactors), relatively-low production costs, and the potential for reduced greenhouse gas emissions [3,5]. Lignocellulose biomass is a viable feedstock that can potentially meet the demands of the European Union's economy for sustainable aviation fuels [8]. However, the economic viability and environmental performance of these processes hinge on the careful management of production costs and biomass utilization efficiency. Optimization efforts must prioritize both energy and carbon efficiencies to mitigate costs and maximize fuel output from biomass resources.

1.1. Biomass-to-liquid (BtL)

Processes that convert biomass into energy-dense liquid fuels are known as biomass-to-liquid (BtL) processes, encompassing a range of products that include methanol and Fischer–Tropsch products, amongst others [5]. These processes typically involve biomass pre-treatment followed by gasification using either fixed bed, fluidized bed, or entrained flow gasifiers (EFG). Subsequently, the syngas's H_2/CO ratio is adjusted *via* the WGS process, and impurities such as tars, ash, and acid gases are removed. Finally, the cleaned syngas is converted into the desired product. A simplified block flow diagram of a BtL process is shown in Fig. 1.

The pre-treatment of biomass aims to optimize its suitability for gasification. Various pre-treatment techniques, including drying, hydrothermal carbonization, torrefaction, pyrolysis, milling, and grinding, are employed to reduce moisture content, improve the carbon-to-oxygen ratio and lower heating value (LHV), and reduce particle size to meet gasifier requirements [5]. In the gasifier, solid pre-treated biomass reacts with an oxidizer, such as steam, air, or oxygen, typically provided by a cryogenic air separation unit, resulting in different gas compositions and temperatures, depending on the gasifier type. The H_2/CO ratio in the syngas, which is crucial for downstream synthesis processes, is often below the stoichiometric ratio required for methane (H_2/CO = 3), methanol (H_2/CO ≈ 2), or FT synthesis (H_2/CO ≈ 2) [5,9]. The WGS reaction

$$CO + H_2O \leftrightarrow CO_2 + H_2 \quad (1)$$

is employed to adjust this ratio, converting steam and CO into H_2 and CO_2 without additional energy input [5,10]. However, this process leads to significant CO_2 losses during subsequent gas conditioning, resulting in low carbon efficiencies in BtL processes.

Prior to synthesis, syngas conditioning is crucial for improving process conditions and preventing catalyst poisoning [5]. For instance, water removal, raw gas reforming, and acid gas cleaning (AGC) are performed to reduce moisture, tar, and sour gas content in the syngas, enhancing its suitability for downstream synthesis processes. Further details on syngas conditioning can be found in Refs. [5,11–14]. In the synthesis step, the syngas is converted into liquid fuels either directly *via* FT synthesis or indirectly *via* the methanol-to-olefins pathway [4,5,15]. Given the technological maturity of the FT process [5] and the suitability of FT products as aviation fuels, the current study focuses on processes utilizing FT synthesis.

1.2. Power- and biomass-to-liquid (PBtL)

Due to the WGS reaction employed in BtL processes, a substantial amount of carbon monoxide undergoes conversion to carbon dioxide,

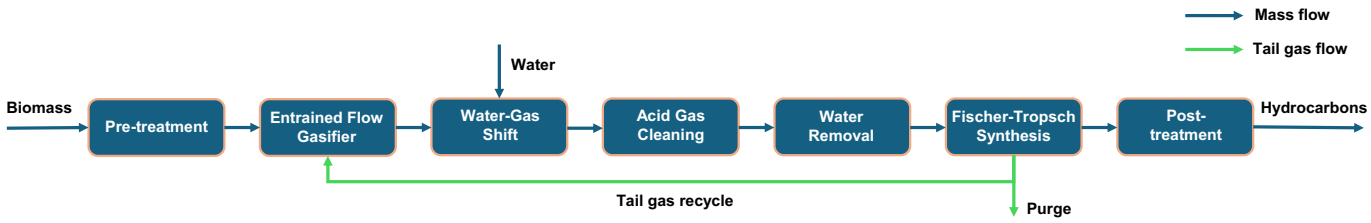

Fig. 1. Simplified block flow diagram of a biomass-to-liquid (BtL) process, using an entrained flow gasifier (EFG) and Fischer–Tropsch (FT) synthesis.

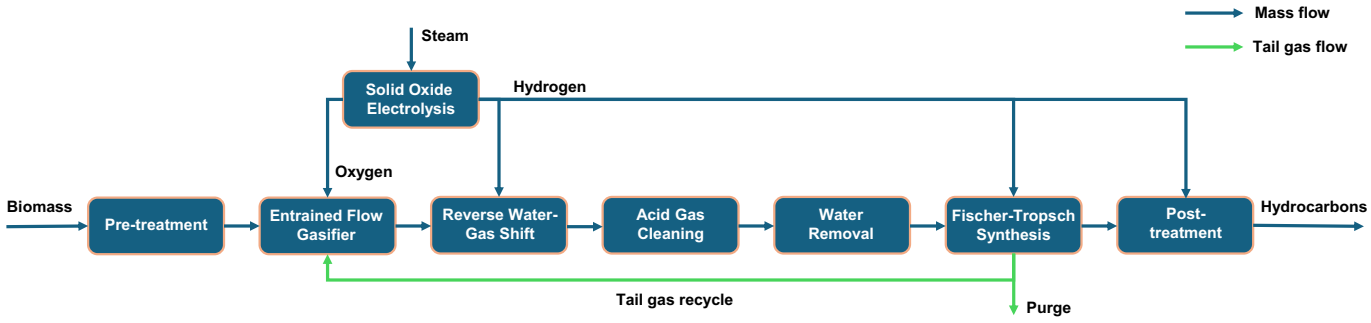

Fig. 2. Simplified block flow diagram of a power- and biomass-to-liquid (PBtL) process that integrates solid oxide electrolysis.

resulting in significant carbon loss during AGC. However, given the limited availability of biomass, achieving high carbon conversion into fuel is paramount for extensive defossilization of the long-haul transport sector [16–18], since 80 % of CO_2 emissions from the aviation sector stem from flights above 1500 km. This objective is attainable through hydrogen production *via* steam electrolysis that is powered by renewable electricity (see Fig. 2). Such integration holds potential to increase the carbon efficiency by a factor of 2–3 by reversing the WGS reaction (reverse water gas shift, RWGS), thereby increasing the production of CO from CO_2 [3,7,8,12,16–20]. Additionally, the introduction of electrolysis cells yields another beneficial outcome: the generation of oxygen during the electrolysis process renders the air separation unit from the BtL process redundant [9]. Surplus oxygen may even be monetized, contributing to the economic viability of the process. Given its potential for significantly higher carbon efficiencies, PBtL processes have gained considerable attention in recent years.

Among the first works discussing the incorporation of hydrogen in PBtL processes, there are the studies conducted by Baliban et al. [12] and Seiler et al. [16]. Baliban et al. explored a combined power-, coal-, biomass-, and natural gas-to-liquid process, while Seiler et al. studied approaches to increase the fuel output of the FT-based PBtL process. Both studies highlighted the significant enhancement in carbon conversion achieved through hydrogen addition to their respective processes, with competitive pricing being attainable. Baliban et al. reported nearly 100 % carbon conversion and identified sufficient national feedstock availability capable of meeting the entire transportation sector's needs in the United States. In contrast, Seiler et al. demonstrated that PBtL processes could satisfy approximately 40 % of France's transportation sector demand with biomass-derived fuels sourced locally. These early investigations underscored the potential of PBtL processes in defossilizing transportation sectors and raised research interest.

Various studies have conducted assessments of the sustainability of PBtL processes, concluding that GHGE from PBtL processes are lower in comparison to BtL and PtL processes [17,21], although they are highly dependent on GHGE from electricity production. Bernical et al. [17] established a threshold of 150 $g_{CO2,eq}$/kWh for their PBtL process to exhibit lower emissions than the reference BtL process, a threshold not yet met by the German electricity mix [22]. However, achieving this threshold is feasible with the utilization of wind, solar, geothermal, and hydro power generation, which have lower specific GHGE [23].

In subsequent studies, PBtL process concepts have been studied in more detail. While fixed bed gasifiers [8,13] and circulating fluidized bed gasifiers [12,24] have been considered, the majority of investigations have favored EFGs due to their high capacities and efficient tar conversion [5]. Moreover, the elevated outlet temperatures of EFGs complement the integration of solid oxide electrolysis cells (SOECs) exceptionally well, because the high-temperature heat that can be recovered during syngas stream quenching can be utilized to produce the steam necessary for SOEC operation. SOEC systems require lower electrical inputs by leveraging the thermal energy present in the steam, thus garnering significant attention in PBtL studies [3,7,8,17,18,25,26]. Consequently, only a handful of studies have explored the viability of polymer electrolyte membrane electrolysis cells (PEM) [7,15,27] and alkaline electrolysis cells [24] as alternatives. Notably, the literature has highlighted the reduced energy efficiency of both PEM [7] and alkaline electrolysis [8].

Despite the considerable attention that PBtL processes have drawn, the majority of investigations have relied on process simulation models. To date, only one experimental project, known as "wind-diesel", has been conducted [19,20]. In a first publication [19], the process exhibited favorable operational characteristics, with the potential for increased FT-liquid output through additional hydrogen supplementation. Both publications highlight the importance of the catalyst selected for process performance.

The economics of PBtL processes have emerged as a focal point in numerous studies, recognized as a primary determinant of their success [27]. Albrecht et al. [27] proposed a framework for techno-economic evaluations, aiming to enhance the comparability of different PBtL studies. Key cost drivers identified include the price of the electrolysis cells and electricity [8]. While PBtL processes may hold an advantage over BtL processes if electricity costs fall below a certain threshold, their competitiveness with conventional fuels remains

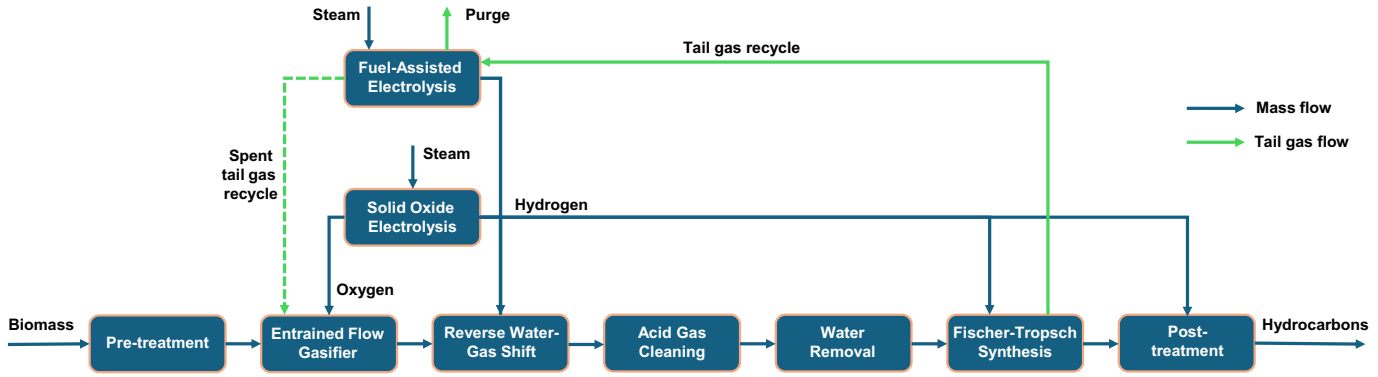

Fig. 3. Simplified block flow diagram of the fuel-assisted power- and biomass-to-liquid (FAPBtL) process. The dashed, green arrow shows the recycle of spent FT tail gas in the recycle variation of the FAPBtL process ($FAPBtL_{recycle}$), and the solid, green purge arrow illustrates the $FAPBtL_{purge}$ variation. (For interpretation of the references to colour in this figure legend, the reader is referred to the web version of this article.)

uncertain and contingent upon further enhancements to process efficiency, as well as escalating emission prices that increase the cost of fossil fuels [3,8,18,21]. In a bid to mitigate fuel production costs, several studies have explored hybrid BtL-PBtL processes to adapt to fluctuating renewable electricity availability [13,19,20,24]. Incorporating electrical energy into the gasification process *via* electrically heated steam has demonstrated beneficial outcomes [26]. Nielsen et al. [28,29] suggested that supplying FT tail gas to the anode of solid oxide electrolysis cells (fuel-assisted SOEC, FASOEC) instead of air could substantially reduce the reversible cell potential and the electricity demand for hydrogen production (see Sections 1.3 and 2.2.8), thus promoting the economic feasibility of PBtL processes. However, a detailed process model of such a system is required to confirm the potential advantages of integrating FASOECs in PBtL processes.

Building upon the foundational contributions of these studies to PBtL process research and development, ongoing efforts are necessary to enhance both energy and carbon efficiencies with the aim of reducing the costs associated with FT fuels. The PBtL process using FASOECs proposed by Nielsen et al. [28,29] holds significant promise for enhancing energy efficiency, but the absence of a detailed model for this process remains a critical gap in our current understanding of how FASOECs influence carbon efficiency and economic feasibility. Additionally, several studies have investigated the influence of fluctuating electricity availability on the PBtL process [13,19,20,24], yet none have explored the adjustment of the WGS equilibrium as a way of tackling these fluctuations. Both of these novel process concepts are described in detail below.

1.3. Fuel-assisted power- and biomass-to-lquid (FAPBtL)

The fuel-assisted PBtL (FAPBtL) process proposed by Nielsen et al. [29] is based on the reference PBtL process developed by Hillestad et al. [3]. However, in the FAPBtL case, the FT tail gas (composed mainly of a mixture of H_2, CO, and CH_4) replaces the conventional inlet flow of air and is redirected to the SOEC anode, where it undergoes electrooxidation. This process harnesses the chemical energy within the FT tail gas to further reduce the electrical energy demand of the electrochemical production of hydrogen in the FASOECs [28,29]. This phenomenon has been observed in previous experiments, where voltage reductions by as much as 1 V have been reported [30–32]. Further, other studies have demonstrated the capability of FASOECs to generate hydrogen and electricity, simultaneously [33–37]. Subsequently, the gas from the anode outlet, with only a small portion that must be purged, can be fed into the EFG to minimize carbon losses ($FAPBtL_{recycle}$). Alternatively, the entire outlet gas from the anode can be purged, as it is depleted of energy ($FAPBtL_{purge}$). However, in the latter process configuration, a significant loss of carbon would be incurred. Fig. 3 illustrates both variations of the FAPBtL process.

1.4. Purge-to-fuel (Purge-tF)

In this analysis, we investigate an additional process case, namely Purge-to-Fuel (Purge-tF), which is a close adaptation of the FAPBtL process. In the PBtL reference case, the purge stream is directed to a fired heater, in order to prepare the steam required by the SOECs. However, it might be possible to provide the required heat for steam preparation from the RWGS outlet stream. In this case, the purge stream could be used in the FASOECs, thereby possibly reducing the required electrical energy in the electrolysis cells. A block flow diagram of Purge-tF process configuration is shown in Fig. 4.

1.5. WGS-adjusted PBtL (WGS-adj)

The advantage of a PBtL process over a BtL process is the increased carbon efficiency. However, this comes at the price of increased electricity consumption, as hydrogen is produced *via* electrolysis. As mentioned previously, there are no studies investigating the effect of an adjusted WGS equilibrium on the PBtL process to deal with fluctuating electricity availability. An adjusted WGS equilibrium could adapt to fluctuating electricity availability by reducing the specific electricity requirement (*i.e.*, less electrical energy per amount of produced fuel), but this would come at the expense of an increased loss of carbon. Nevertheless, this adjustment could provide more flexibility in the operation of the process in order to make it more economically viable. Additionally, PBtL processes with adjusted WGS equilibrium could be more comparable to FAPBtL processes. It is expected that $FAPBtL_{recycle}$ processes exhibit a similar carbon efficiency to the reference PBtL process, as the same amount of (depleted) FT tail gas is reintroduced into the EFG. Thus, the $FAPBtL_{recycle}$ process configuration should be readily comparable to the PBtL reference case by assessing their respective energy requirements. However, in the $FAPBtL_{purge}$ scenario, the carbon efficiency is expected to decrease significantly due to the absence of the recycle to the EFG, making the comparison to the reference case more challenging. Nonetheless, if the RWGS reaction were mitigated or even reversed to a standard WGS reaction, the process would require less hydrogen at the expense of reduced carbon efficiency as for the FAPBtL process. Achieving a reduced RWGS reaction entails directing hydrogen to the FT reactors, while a subsequent reintroduction of the WGS reaction involves adding steam to the WGS reactor. This approach could serve as a competitive alternative to the $FAPBtL_{purge}$ scenario and is thus also modelled to determine the viability of the $FAPBtL_{purge}$ process in the ongoing development of PBtL processes. Fig. 5 presents a simplified block flow diagram of the WGS-adjusted PBtL process. In this study, this process configuration is referred to as WGS-adj.

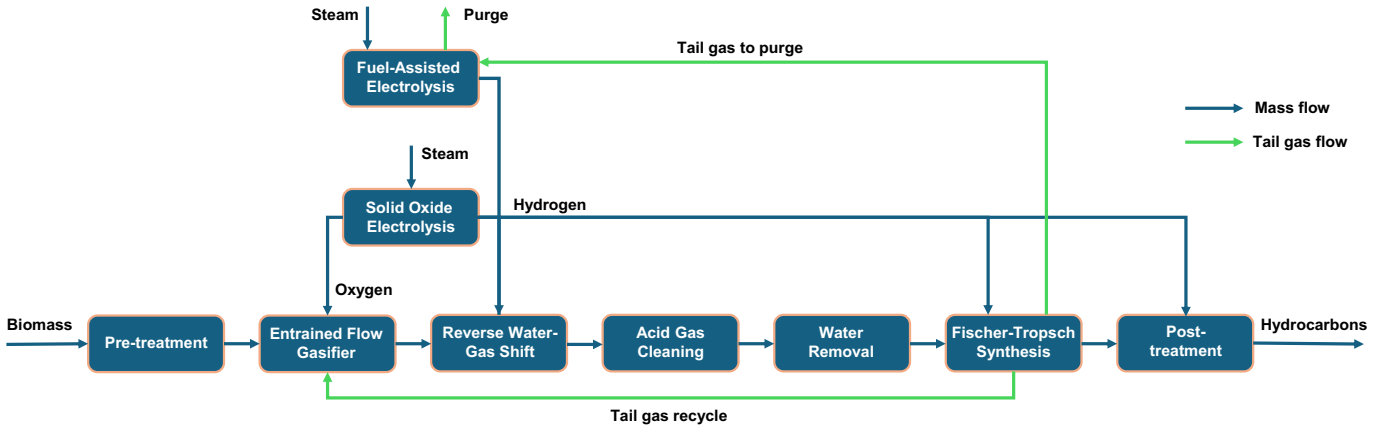

Fig. 4. Simplified block flow diagram of the Purge-to-Fuel (Purge-tF) process configuration. The purge stream is sent to the fuel-assisted solid oxide electrolysis cells (FASOECs) before being purged.

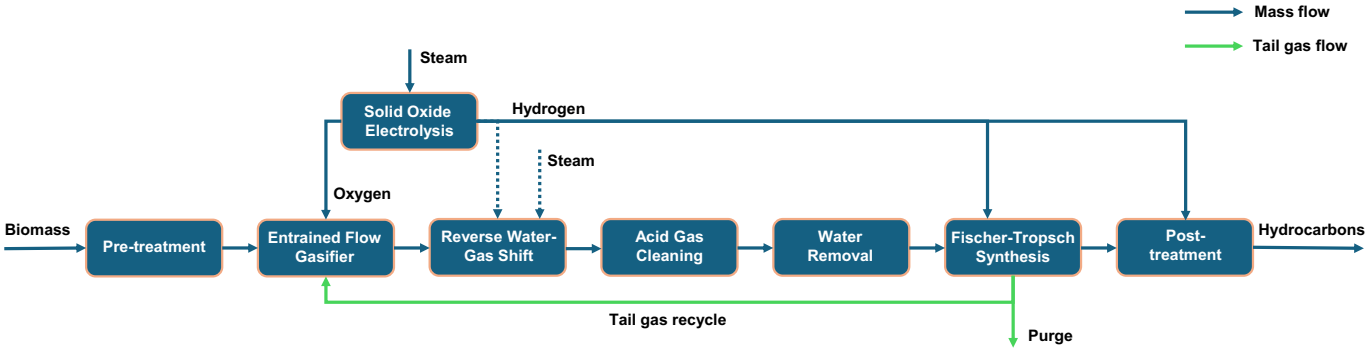

Fig. 5: Simplified block flow diagram of a PBtL process with an adjusted WGS equilibrium (WGS-adj). To reduce the RWGS reaction, the amount of hydrogen fed to the RWGS reactor is reduced (dashed hydrogen arrow). When no hydrogen is fed to the RWGS reactor, steam can be fed to the WGS reactor (dashed steam arrow) to further reduce the hydrogen requirements of the process.

1.6. Objectives and outline

As described above, both carbon conversion and energy consumption in PBtL processes are pivotal for their viability in replacing fossil fuels within the long-haul transport sector. High carbon efficiencies are essential to ensure a sustainable utilization of biomass feedstock and to meet the fuel demand of this sector. Increasing the carbon efficiency appears feasible through green hydrogen addition, thereby shifting the equilibrium of the WGS reaction from CO_2 to CO and increasing the amount of carbon available for FT synthesis. However, hydrogen production via electrolysis entails increased electricity demand, leading to higher costs. Consequently, this study strives to contribute to the ongoing advancement of PBtL processes by identifying improved process configurations that achieve both reduced energy demands and increased carbon efficiencies. Three novel process concepts have been presented above, namely fuel-assisted power- and biomass-to-liquid (FAPBtL), water gas shift-adjusted PBtL (WGS-adj), and Purge-to-Fuel (Purge-tF), all of which are investigated herein. Notably, most of the process concepts with a few adaptations could also be applied to PtL processes that use carbon dioxide instead of biomass as carbon source. However, investigating PtL processes is beyond the scope of the current study.

This study first constructs and validates a PBtL process model using the results reported by Hillestad et al. [3]. Subsequently, this PBtL model is adapted to include the modifications necessitated by the FAPBtL (both $FAPBtL_{recycle}$ and $FAPBtL_{purge}$), WGS-adj, and Purge-tF processes. For each of these process models, we evaluate carbon, mass, and energy balances (heat, chemical, and electrical energies) to compare carbon and energy efficiencies across different process configurations. We then conduct an economic analysis to compare the modelled configurations and determine the most cost-competitive.

The remainder of this work is organized as follows: Section 2 contains a detailed description of the process models, while Section 3 describes the model validation, followed by mass, carbon, energy, and techno-economic analyses, along with a comparison of the results of the different process cases. In Section 4, conclusions and outlook are provided.

2. Model development

Aspen HYSYS V12.1 was employed as the modelling software, utilizing the Peng–Robinson equation of state. The biomass considered in this work is modelled as a pseudocomponent following the description from Hillestad et al. [3], and it is characterized by the pseudomolecule $C_{4.31}H_{6.04}O_{2.624}N_{0.012}S_{0.003}$ and has a molecular weight of 100.11 g/mol and a heat of formation of -5.1846×10^5 kJ/kmol. A constant wet biomass flow of 87.5 t/h (including a 5 wt% moisture content) is used in all cases, according to the reference case [3]. A comprehensive model for all process configurations is developed, and the various process steps are modelled in sub-flowsheets and integrated into the top-level flowsheet. Details of the top-level flowsheet are provided in Section 2.1, while the sub-flowsheets are described in Section 2.2. Finally, the key assumptions for the techno-economic analysis and their corresponding references are reported in Section 2.3.

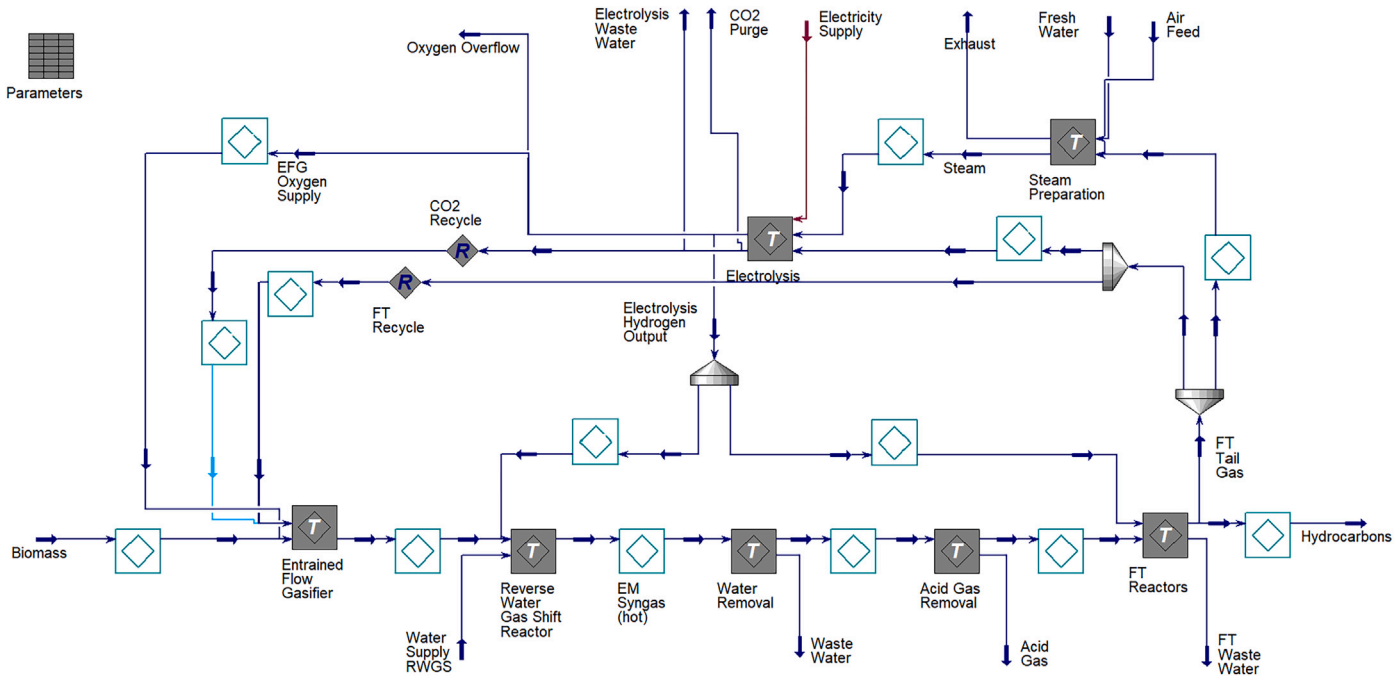

Fig. 6. Screenshot of the top level flowsheet of the combined process model in Aspen HYSYS. Sub-flowsheets are shown as gray squares with a "T" in the middle, energy measurement sub-flowsheets are shown as wire-frame objects with white fillings, and diamonds with an "R" are recycle blocks that are required for solving the process model numerically. (For interpretation of the references to colour in this figure legend, the reader is referred to the web version of this article.)

2.1. Process model

As shown in Figs. 2–5, the different processes investigated in this work are similar in most aspects, differing primarily in the utilization of the FT tail gas and the amount of hydrogen/steam supplied to the (R)WGS reactor. Consequently, a unified model for all process variations is developed. Fig. 6 presents a screenshot of the Aspen HYSYS model's flowsheet. For enhanced readability, the sub-processes have been grouped into sub-flowsheets, the details of which are provided in Section 2.2. Energy calculations are performed for all streams on the main flowsheet, apart from those that do not contain chemical or thermal energy. These energy calculation sub-flowsheets are depicted as wire-frame objects (white filling), which serve solely for computation purposes and do not affect the connected streams in the actual process.

In the depicted flowsheet, the biomass is introduced into the *Entrained Flow Gasifier* sub-flowsheet, where it undergoes oxygen-based gasification. The resulting syngas is then transferred to the *Reverse Water Gas Shift Reactor* sub-flowsheet, where the equilibrium of the WGS reaction and the hydrogen demand are determined. In the WGS-adj scenario, steam instead of hydrogen may be introduced in this unit. Subsequently, the syngas proceeds to the *Water Removal* sub-flowsheet for drying before being directed to the *Acid gas cleaning* sub-flowsheet. Here, sulfuric components and the majority of the remaining CO_2 in the syngas are removed. The purified syngas is then fed into the *FT Reactors* sub-flowsheet, where it is converted in a three-stage FT reactor. The FT reaction products, including water, hydrocarbons, and tail gas, are then separated. The FT tail gas undergoes two splits. In the first split, a portion of the FT tail gas may be diverted as a purge to prevent the accumulation of inerts in the system. This purge stream is routed to the *Steam Preparation* sub-flowsheet, where it is combusted to generate heat for steam production used in the electrolysis process. In the second split, the remaining FT tail gas is either returned to the *Entrained Flow Gasifier* sub-flowsheet (in the PBtL and WGS-adj cases and partly in the Purge-tF case) or directed to the *Electrolysis* sub-flowsheet (in the FAPBtL and partly in the Purge-tF case). Within the *Electrolysis* sub-flowsheet, calculations for electrolysis are performed, encompassing both conventional and fuel-assisted SOECs. The produced hydrogen is distributed to the (R)WGS reactor and the FT reactors based on their respective requirements calculated in their sub-flowsheets. Moreover, the oxygen needed for gasification is produced from the conventional SOECs; any excess oxygen is routed to an overflow stream. Table 1 provides an overview of the key parameters that distinguish the various models. Across all scenarios, 8.8 % of the FT tail gas is purged, either through the steam preparation process or *via* the FASOECs.

2.2. Sub-processes

2.2.1. Biomass pre-treatment

To prepare the biomass for the PBtL process, various pre-treatment methods such as drying, hydrothermal carbonization, torrefaction, pyrolysis, milling, and grinding can be employed [5]. For the reference process in this study, Hillestad et al. [3] determined that biomass drying, torrefaction, and milling are necessary. The drying process reduces the water content of the biomass from 40 wt% to 5 wt%, requiring a significant amount of heat of 2.8 MJ/kg at 150 °C. With an input of 83.3 t/h of dry biomass, the heat requirement is 18.5 MW. In the torrefaction process, the biomass reacts with an under-stoichiometric amount of oxygen, improving its grindability [38,39]. The tail gas from the torrefaction process is fed into the EFG. Torrefaction requires both heat and oxygen. Subsequently, the torrefied biomass is ground to achieve a small particle size of about 0.5 mm, which is essential for optimal conversion in the EFG [3,40]. The pre-treatment process is not considered in this work, however, the availability of heat for the drying process is explored in Section 3.3.

2.2.2. Entrained flow gasifier (EFG)

In the EFG, the pre-treated biomass undergoes gasification through the introduction of oxygen. The oxygen flow rate is adjusted to achieve a temperature of 1600 °C and understoichiometric conditions [3]. This elevated temperature is necessary to facilitate the thermal cracking of tars and the melting of ashes, leading to increased production rates of hydrocarbons and carbon monoxide, as well as simplified gas cleaning

Table 1
Key model parameters to differentiate the PBtL, FAPBtL (FAPBtL$_{purge}$ and FAPBtL$_{recycle}$), WGS-adj, and Purge-tF process configurations based on FT tail gas usage and FASOEC anode tail gas usage.

	Process configuration	PBtL	FAPBtL	WGS-adj	Purge-tF
FT tail gas usage	Steam preparation	8.8 %	0 %	8.8 %	0 %
	EFG	91.2 %	0 %	91.2 %	91.2 %
	FASOEC	0 %	100 %	0 %	8.8 %
	RWGS H_2 bypass ratio	0 %	0 %	0 %-100 %	0 %
	WGS steam feed rate	0 kg/h	0 kg/h	≥0 kg/h	0 kg/h
	FAPBtL sub-process configuration		FAPBtL$_{purge}$	FAPBtL$_{recycle}$	Purge-tF
FASOEC anode tail gas usage	EFG		0 %	91.2 %	0 %
	Purge		100 %	8.8 %	100 %

processes [41,42]. In Aspen HYSYS, the EFG is modelled using two reactors, as shown in Appendix A, Supplementary Fig. A1. The first reactor is a conversion reactor, where the biomass is decomposed into its elemental constituents, requiring the heat of formation as an energy input. This energy is supplied by the second reactor, where the elemental biomass components react with O_2 until thermodynamic equilibrium is attained (modelled as a Gibbs reactor). The EFG is assumed to be adiabatic as its large volume renders specific heat losses negligible; therefore, the sum of the heat streams from the two reactors equals zero. An adjustment block regulates the oxygen supply to maintain the outlet temperature at 1600 °C.

2.2.3. (Reverse) water gas shift ((R)WGS) reactor

At the outlet of the EFG, the syngas typically contains more than 5 mol% CO_2. This poses a challenge to carbon efficiency, as most of the CO_2 is removed in the AGC unit, thus being lost. To mitigate this loss of CO_2, hydrogen is added to the syngas to promote the RWGS reaction (see Eq. 1). In the RWGS reactor, CO_2 reacts with H_2 to form CO. According to calculations by Hillestad et al. [3], the high temperature of the syngas facilitates rapid reaction kinetics, thereby avoiding the need for a catalyst to achieve thermodynamic equilibrium in the RWGS reactor. In Aspen HYSYS, the RWGS reactor is modelled with an equilibrium reactor (*i.e.*, a Gibbs reactor) as illustrated in Appendix A, Supplementary Fig. A2. The addition of H_2 is regulated by an adjustment block, ensuring that H_2 is introduced to the RWGS reactor until a H_2/CO ratio of 2.05 is obtained at the outlet of the RWGS reactor. In the WGS-adj case, a hydrogen stream is combined with the EFG products and possibly steam. The gas effluent from the Gibbs reactor is then mixed with the hydrogen bypass stream. Although no liquid products are generated at the current operating conditions, a liquid stream is added as required by the Gibbs reactor block.

2.2.4. Water removal

In the water removal sub-flowsheet (see Appendix A, Supplementary Fig. A3), the hot syngas stream is cooled to 40 °C to condense the contained water. Subsequently, the liquid fraction of the stream is separated and discarded, effectively eliminating water from the syngas stream.

2.2.5. Acid gas cleaning (AGC)

The AGC process is required to eliminate sulfuric components from the syngas, which could otherwise poison the catalysts in the Fischer–Tropsch reactors [3,24]. This removal is modelled as a component splitter (see Appendix A, Supplementary Fig. A4), designed to extract all sulfuric components along with 90 % of the CO_2 from the syngas stream [3]. The carbon efficiency could be improved by recycling a portion of the extracted components back to the (R)WGS reactor [24].

2.2.6. Fischer–Tropsch (FT) synthesis

In the FT reactors, the syngas undergoes a series of reactions to produce liquid fuels. In these reactors, carbon monoxide reacts with hydrogen to form paraffins, olefins, and oxygenates, as described by the following reactions, respectively:

$$nCO + (2n+1)H_2 \rightarrow C_nH_{2n+2} + nH_2O \quad (2)$$

$$nCO + 2\,nH_2 \rightarrow C_nH_{2n} + nH_2O \quad (3)$$

$$nCO + 2\,nH_2 \rightarrow C_nH_{2n+2}O + (n-1)H_2O. \quad (4)$$

However, due to the low generation of oxygenates, their contribution is typically negligible and therefore neglected in the Fischer–Tropsch synthesis process model [3].

For FT synthesis, slurry bubble column reactors are commonly employed due to their selectivity towards olefins and higher hydrocarbons, as well as their low WGS activity [3,10]. These reactors can be effectively modelled as continuous stirred tank reactors (CSTR) [3]. Ostadi et al. [43] have provided a detailed model for the stoichiometry and kinetics based on experimental data from Todic et al. [44] for a CSTR configuration. The reaction stoichiometry in this model follows the Anderson–Schulz–Flory (ASF) distribution, which depends on the chain growth factors α_i, where i represents the reaction number (1 for paraffins and 2 for olefins). These reactions can be expressed as

$$CO + \nu_{1,H_2}H_2 \xrightarrow{r_1} \sum_{n=1}^{\infty} \nu_{i,n}C_nH_{2n+2} + H_2O, \quad (5)$$

and

$$CO + \nu_{2,H_2}H_2 \xrightarrow{r_2} \sum_{n=1}^{\infty} \nu_{i,n}C_nH_{2n} + H_2O, \quad (6)$$

with stoichiometric coefficients $\nu_{i,n}$ given in Appendix A, Supplementary Table A1.

The stoichiometric coefficients have been calculated according to the model developed by Todic et al. [44] and Ostadi et al. [43], which is also detailed in Appendix A, Supplementary Note 1, Eqs. A1–A13. It should be noted that these coefficients depend on the chain growth factor, which itself relies on the syngas composition and temperature. However, Aspen HYSYS cannot model a variable chain growth factor directly. Consequently, constant chain growth factors of $\alpha_1 = 0.93$ and $\alpha_2 = 0.71$, as proposed by Agazzi [45], are used in this study. For short-to-medium C-chain paraffins and short C-chain olefins, the individual components were considered for simulation. In contrast, a paraffin lump component, containing all paraffins with a carbon number higher than 21, and an olefin lump component, containing all olefins with a carbon number higher than 6, are introduced. Characteristics of these lump components are presented in Table 2.

Table 2
Characteristic values for paraffin and olefin lump components according to Agazzi [45] and calculated according to Eq. (9).

	Paraffins (C21+)	Olefins (C6+)
Smallest carbon number	21	6
Mean carbon number	34.29	8.45
Molecular weight (kg/mol)	482.88	118.48
Boiling point (°C)	484.0	133.3
Higher heating value (MJ/kg)	46.8	46.4

Table 3
Fischer–Tropsch reaction rate parameters for the *Heterogeneous Catalytic Reaction* model in Aspen HYSYS, according to [45].

	Paraffin formation	Olefin formation	Methanation
A	4.1460×10^{11}	3.3168×10^{10}	1.3707×10^{13}
E (kJ/kmol)	86,102	86,102	1.1292×10^{5}
β	0	0	0
n	3	3	3

According to Refs. [3] and [43], the observed methane production rate exceeds the predictions of the ASF distribution. Hence, an additional methanation reaction is introduced:

$$CO + 3\,H_2 \xrightarrow{r_3} CH_4 + H_2O \tag{7}$$

The stoichiometric coefficients for the three modelled reaction sets and their kinetics are provided in Appendix A, Supplementary Table A1 and Supplementary Note 1, Eqs. A10–A13. In Aspen HYSYS, the *Heterogeneous Catalytic Reaction* environment is used to model the reactions, and the factor $k\,(T)$ is calculated as

$$k(T) = A \exp\left(\frac{-E}{RT}\right) T^{\beta}, \tag{8}$$

with A and β denoting the kinetic parameters, R denotes the universal gas constant, and T represents temperature. Hillestad et al. [3] did not specify the catalyst concentrations, while Agazzi [45] calculated the kinetic parameters for a catalyst concentration of 200 kg m^{-3}. However, the kinetic factor A calculated by Agazzi is approximately 200 times higher than the value given by the model from Ostadi et al. [43], which fits the data from Todic et al. [44] for a concentration of 14 kg m^{-3}. Therefore, the kinetic factor A calculated by Agazzi should only be 200/14 times higher than the one calculated by Todic et al., but for the sake of comparability and since this adjustment primarily affects the reactor sizes, the kinetic values used by Agazzi are retained in this work and can be found in Table 3. To analyze the energy flows of the PBtL process, it is necessary to calculate the higher heating values of the alkane and alkene lump components. Demirbas et al. [46] proposed the equation:

$$HHV = 0.303 w_C + 1.423 w_H, \tag{9}$$

where w_C and w_H are the weight fractions of carbon and hydrogen in wt%, respectively.

In Appendix A, Supplementary Fig. A5, a screenshot of the FT subflowsheet is shown. The syngas undergoes the three-stage FT reactor and, after each reactor stage, the products are separated into gas, water, and hydrocarbons, in a flash. Additional hydrogen is fed to the reactor stages 2 and 3 to reach the required H_2/CO ratio. A screenshot of the second stage is shown in Appendix A, Supplementary Fig. A6. After the addition of the supplementary H_2, the syngas is heated to 210 °C and fed to the CSTR. The reactor size is designed such that the CO-conversion within the stage is 55 % [3]. In the last step, the products are split into the gaseous, light liquid (hydrocarbons), and heavy liquid (water) phases. It should be noted that CO_2 hydrogenation is not considered in the FT reactors, since the catalyst used in this study does not facilitate this reaction [43,44]. Nevertheless, implementing a FT reactor with a catalyst that promotes CO_2 hydrogenation represents a compelling route for additional CO_2 conversion [47], but is beyond the scope of the current study.

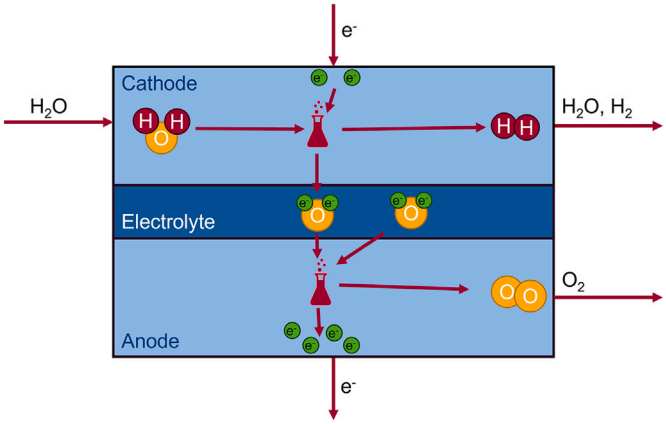

Fig. 7. Illustration of the electrolysis process in an SOEC. Steam is fed into the cathode, where the application of a current splits water molecules into hydrogen and O^{2-} ions. Excess steam and the produced hydrogen are then released at the cathode outlet. The O^{2-} ions produced in the cathode travel through the electrolyte into the anode, where they release electrons and form oxygen that is released at the anode outlet.

2.2.7. Solid oxide electrolysis cells (SOECs)

SOECs represent a promising technology in hydrogen production. Within SOECs, steam is directed to the cathode, where it undergoes splitting into H_2 and O^{2-} ions upon the application of a current. These O^{2-} ions are then transported through the solid oxide electrolyte and evolve into O_2, concurrently releasing their excess electrons to the anode. This process is illustrated in Fig. 7. Operating at elevated temperatures, SOECs exhibit high efficiency, potentially requiring only half the electric power compared to low-temperature electrolysis cells owing to their capability to harness waste heat [28]. In this study, the SOECs are assumed to be adiabatic and operated thermoneutrally at 40 bar and 850 °C, in accordance with Hillestad et al. [3]. In Aspen HYSYS, the SOEC is modelled as a conversion reactor, incorporating a steam utilization factor of $U_{SOEC} = 0.8$. Given a specified hydrogen production rate $\dot{n}_{H_2}$ and steam utilization, the required steam feed flow $\dot{n}_{H_2O}$ can be calculated as

$$\dot{n}_{H_2O} = \frac{\dot{n}_{H_2}}{U_{SOEC}}, \tag{10}$$

and the oxygen molar flow rate $\dot{n}_{O_2}$ from the SOEC can be determined by

$$\dot{n}_{O_2} = \frac{1}{2}\dot{n}_{H_2O}. \tag{11}$$

The electrical power demand is subsequently computed by the conversion reactor.

2.2.8. Fuel-assisted solid oxide electrolysis cells (FASOECs)

The FASOECs operate by introducing fuel (such as CO, CH_4, or H_2 from the FT tail gas) instead of air into the anode of a cell, thus preventing the production of oxygen in the anode. This arrangement allows oxygen ions to react electrochemically with the fuel present in the anode, thereby reducing the electrical energy required in the electrolysis reaction. An illustration of this process is shown in Fig. 8. This integration of fuel into the anode of the SOECs can significantly reduce the electrical power required for electrolysis [28,29].

In this study, the computational model developed by Nielsen et al. [29] is utilized, and all details concerning material selection, cell

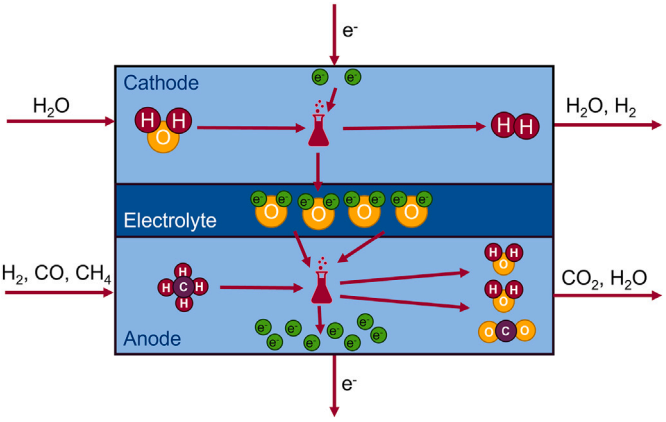

Fig. 8. Illustration of the electrolysis process in a FASOEC. Steam is fed into the cathode, where the application of a current splits water molecules into hydrogen and O^{2-} ions. Excess steam and the produced hydrogen are then released at the cathode outlet. The O^{2-} ions produced in the cathode travel through the electrolyte into the anode, where they react electrochemically with the provided fuel, shown here as CH_4 as an example. Reactions with CO and H_2 occur analogously.

specifications, and computational modelling can be found in Ref. [29]. The FASOECs and SOECs consist of a Ni-YSZ anode, a YSZ electrolyte, and an LSM-YSZ cathode, which are some of the most commonly used materials in commercial SOEC applications and are the reason they are selected [48]. The chosen cell dimensions are a 40 cm × 40 cm active electrode area [49,50] with a channel height of 1 mm [51], and the current density is selected to range between i_{min} = 2.25 A cm^{-2} and i_{max} = 2.5 A cm^{-2} [29]. It should be noted that FASOECs have been shown to attain current densities of over 3.0 A cm^{-2} [52]. The assumed lifetime of both FASOECs and SOECs considered in this work is 50,000 h, which is within the range of current technology and future prospects [48].

The Fischer–Tropsch tail gas contains mainly H_2, CH_4 and CO (other components are below 1 mol%, with nitrogen being inert). The FASOEC model developed by Nielsen et al. [29] models the utilization of H_2, CH_4 and CO, therefore, the remaining components are bypassed into the anode outlet and neglected in the FASOEC calculations. The addition of these components to the FASOEC calculations is expected to further reduce the operating potential of the FASOECs, but due to the lack of the FASOEC model's capability to calculate the utilization of other components, this effect could not be included in this study. The validity of this simplification should be verified once a FASOEC model including the utilization of higher hydrocarbons is available. The H_2 production rate in the cathode $\dot{n}^{prod}_{H_2}$ of the FASOEC from the provided fuel to the anode can be calculated as

$$\dot{n}^{prod}_{H_2} = U^{fuel}_{\text{FASOEC}} \left(\dot{n}^{fuel}_{H_2} + 4\dot{n}^{fuel}_{CH_4} + \dot{n}^{fuel}_{CO} \right), \tag{12}$$

where $\dot{n}^{fuel}_{H_2}$, $\dot{n}^{fuel}_{CH_4}$ and $\dot{n}^{fuel}_{CO}$ are the component molar flows in the fuel and U^{fuel}_{FASOEC} is the electrochemical utilization of the fuel in the FASOEC. Using the Faraday constant F, the required current for hydrogen production in the FASOEC is calculated as

$$I_{\text{FASOEC}} = 2\, F \dot{n}^{prod}_{H_2}, \tag{13}$$

which then yields the number of FASOECs required in the FAPBtL process

$$n_{\text{FASOEC}} = \frac{1}{2} \left(\frac{I_{\text{FASOEC}}}{I_{min} A_{\text{FASOEC}}} + \frac{I_{\text{FASOEC}}}{I_{max} A_{\text{FASOEC}}} \right). \tag{14}$$

The fuel velocity supplied to the anode inlet is then calculated as

$$v_{fuel} = \frac{\dot{V}_{fuel}}{n_{\text{FASOEC}} A_{\text{FASOEC}}}, \tag{15}$$

where $\dot{V}_{fuel}$ is the actual volume flow rate of the fuel and A_{FASOEC} is the cross-section of the anode channel. The steam velocity to the cathode channel is calculated using an analogous approach.

In the integration process, the steam and fuel inlet velocities, as well as the fuel composition, are used as inputs into the FASOEC Python code developed by Nielsen et al. [29]. An iterative process is then undertaken until the calculated fuel utilization matches the set fuel utilization in the Aspen HYSYS model. The steam utilization and current density calculated by the code are used to validate the results. Upon completion of the iterations, the results from the Python code, including current density, operating potential, fuel utilization, steam utilization, and component utilizations, are transferred back into Aspen HYSYS, and used to calculate the required power and the outlet streams of the FASOECs. A screenshot of the electrolysis sub-flowsheet can be seen in Appendix A, Supplementary Fig. A7.

Based on the process being simulated, hydrogen may be produced by the conventional SOECs or by both the SOECs and the FASOECs. The hydrogen requirement is determined by the (R)WGS reactor and the FT reactors. The FASOECs produce as much hydrogen as possible based on the given fuel feed and fuel utilization. Any additional hydrogen requirement is then produced by the SOECs.

2.2.9. Steam preparation

In the steam preparation sub-flowsheet (see Appendix A, Supplementary Fig. A8), water at ambient conditions is pressurized, heated, evaporated, and superheated to reach the electrolysis inlet conditions of 40 bar and 850 °C. Initially, the water is heated by burning the FT tail gas purge stream (applicable only in the PBtL and the WGS-adj cases). Subsequently, the water is further heated to 850 °C. It is assumed that sufficient heat is available within the required temperature range, which is confirmed in Section 3.3.

2.2.10. Energy flow calculation

In order to visualize the energy flows in the process, a calculation of the energy contained in the mass streams needs to be performed. The reference point for these measurements is chosen to be the completely oxidized products at 25 °C, with water being liquid. The energy content of a stream is therefore the sum of its sensible and latent heat as well as its higher heating value. Aspen HYSYS does not directly calculate this value. Therefore, an *Energy Measurement* sub-flowsheet has been introduced (see Appendix A, Supplementary Fig. A9) to perform this calculation. In this sub-flowsheet, the mass stream is cooled to 25 °C and then reheated to its original temperature. Therefore, the mass stream at the outlet is in the exact same condition as at the inlet, but the sensible heat of the mass stream is yielded as the energy stream released by the cooler. The spreadsheet then calculates the energy flow $\dot{E}$ according to

$$\dot{E} = \dot{Q}_{cool} + \dot{n}\text{HHV} - \dot{n}_{H_2O} \Delta h_{V,H_2O}, \tag{16}$$

where $\dot{Q}_{cool}$ is the heat released by the stream, $\dot{n}$ is the molar flow, HHV is the molar higher heating value, $\dot{n}_{H_2O}$ is the molar flow of the water contained in the stream, and $\Delta h_{V,H_2O}$ is the molar heat of evaporation of water. The term $\dot{n}_{H_2O} \Delta h_{V,H_2O}$ is subtracted because Aspen HYSYS considers all educts as gaseous for the calculation of the higher heating value (HHV). Apart from water, only hydrocarbons could be in a liquid state at 25 °C, however, their heat of evaporation is neglected because it is small compared to their higher heating values.

2.3. Techno-economic model

Albrecht et al. [53] and Maier et al. [54], both from the German Aerospace Center (DLR), developed an in-house techno-economic analysis tool called TEPET. This tool was used to calculate the net production

Table 4
List of basis conditions for the production of liquid synthetic fuels using the PBtL process variants.

Basis conditions	Value
Base year	2023
Basis currency	€
Plant life time	20 a
Full load hours	8,260 h/a
Interest rate	7 %
Plant location	Norway

costs (NPC) of Fischer–Tropsch (FT) fuels for each process configuration studied in this work. Integrated with Aspen HYSYS, TEPET conveniently reflects variations in NPC resulting from changes in process configuration. The key economic metrics evaluated include capital investment expenditures (CAPEX), operational expenditures (OPEX), and NPC, based on the PBtL process variants and assumptions listed in Table 4. All references for equipment cost estimation have been adjusted to consider the present-day cost of the equipment using the Chemical Engineering Plant Cost Index (CEPCI). Further details on the TEPET tool and the economic analysis methodology are available in Refs. [53–55].

2.3.1. Capital investment expenditure (CAPEX)

The fixed capital investment (FCI) costs comprise equipment costs (EC) as well as expenses related to engineering, procurement, and construction. A comprehensive explanation of TEPET's CAPEX evaluation for each configuration is provided in the Supplementary Materials of Ref. [55]. Cost functions for standard equipment, including heat exchangers (boilers and condensers), compressors, pumps, flash drums, and furnaces, are taken from Ref. [56]. Additional information for calculating FCI and annualized capital costs (ACC) is also detailed in the Supplementary Materials of Ref. [55].

2.3.2. Operational expenditure (OPEX)

Operational expenditures are categorized into direct OPEX, covering raw material and utility costs, and indirect OPEX, encompassing maintenance, labor, insurance, and other operational costs. Direct OPEX is calculated from the process simulation results by considering average annual market prices for the selected base year (2023), as shown in the following expression

$$\mathrm{OPEX}_{dir} = \sum_{i=1}^{m} \dot{m}_{R,i} \cdot c_{R,i} + P_{el,eff} \cdot c_{el} - \sum_{k=1}^{p} \dot{Q}_{HM,k} \cdot r_{HM,k}. \quad (17)$$

Eq. (17) accounts for streams crossing system boundaries, including material flows in the form of raw materials or by-products $\dot{m}_{R,i}$, the aggregated electrical power demand $P_{el,eff}$, and heat streams $\dot{Q}_{HM,k}$ multiplied with their respective costs or revenues $c_{R,i}$, c_{el}, and $r_{HM,k}$, with subscript k representing different process configurations. The indirect operational expenditures $\mathrm{OPEX}_{\mathrm{ind}}$, including maintenance and administrative costs, remains consistent across all configurations and is detailed in Tables 5 and 6.

2.3.3. Net production costs (NPC)

The NPC is determined using the following equation

$$\mathrm{NPC} = \frac{\mathrm{ACC} + \sum \mathrm{OPEX}_{\mathrm{ind}} + \mathrm{OPEX}_{\mathrm{dir}} + h_{labor} c_{labor}}{\dot{m}_{fuel}}, \quad (18)$$

where ACC, $\mathrm{OPEX}_{\mathrm{ind}}$, $\mathrm{OPEX}_{\mathrm{dir}}$ have been described above, $\dot{m}_{fuel}$ is the mass flow rate of FT fuel produced, and h_{labor} and c_{labor} denote the amount of hours of labor per year and the cost of labor, respectively, which can be found in Table 6.

Table 5
Ratio factors for the estimation of indirect OPEX for fluid processing plating and the associated costs [56]. M€ corresponds to millions of €.

Investment item	Typical value	Cost per year (M€/y)
Operating supervision	0.15	1.75
Maintenance labor	0.01	28.25
Maintenance material	0.01	28.25
Operating supplies	0.15	8.47
Laboratory charges	0.2	2.33
Insurance and taxes	0.02	56.50
Plant overhead cost	0.6	24.98
Administrative costs	0.25	6.25

Table 6
Operating labor costs for the estimation of indirect OPEX. M€ corresponds to millions of €.

Investment item	Total employee hours per year	Labor costs (€/h)	Cost per year (M€/y)
Operating labor costs	165,200	70.46	11.64

With this techno-economic modelling framework, we can conduct a consistent comparison between the different process configurations modelled in Aspen HYSYS.

3. Results and discussion

The results and discussion section begins with the validation of the PBtL process developed in this study with the work by Hillestad et al. [3], followed by mass and carbon flow analyses, an energy flow analysis, a heat integration analysis, and finally an economic analysis of the considered process configurations.

3.1. Validation of the PBtL process

As mentioned previously, the process models developed in this work are based on the PBtL model by Hillestad et al. [3] and is therefore compared to their results. In the process model for the reference case (PBtL), a dry biomass input flow of 83.3 t/h yields a fuel production rate of 46.2 t/h, corresponding to a carbon efficiency of 91.07 %. These two values differ by approximately 0.3 % from those reported by Hillestad et al. Table 7 presents key values calculated in this work alongside the corresponding values from Hillestad et al.'s reference process, as well as their relative deviations. Most of the calculated values deviate from the reference values by less than 2 %, with a few exceptions. The most notable exception is the FT reactor volume, which is calculated to be 37 % lower in this study compared to the reference value. As discussed in Section 2.2.6, this discrepancy arises because the catalyst concentrations used in the FT reactor were unspecified in Ref. [3]. Further, the molar fraction of CH_4 in the FT tail gas is 6.4 % higher than in the reference case. This discrepancy may be attributed to the assumption of constant chain growth factors in the FT reactions in this study, contrary to the approach by Hillestad et al., likely causing differences in the product distributions. The higher CH_4 content in the tail gas might also explain the increased power requirement of the SOEC (1.8 % above the reference case). With a higher CH_4 content in the tail gas, more hydrogen atoms are lost in the tail gas purge, resulting in a greater hydrogen need and increased power requirement. Finally, the deviation of the CO_2 emissions per produced fuel exceeds 2 %, although the deviation is only 2.6 %. This can be partially explained by the slightly lower fuel production in this study, which means that the released CO_2 is attributed to a smaller amount of fuel.

The CO_2 contents of selected streams are also shown in Table 7. Approximately 75 % of the CO_2 emissions occur during AGC, while the FT tail gas purge accounts for the remaining losses. Since the purge is

Table 7
Comparison between the key performance metrics determined by the PBtL model in the current study and those calculated by Hillestad et al. [3].

Variable	Current work	Value from Hillestad [3]	Relative deviation
CO-conversion per pass (%)	90.93	90.90	0.03 %
Carbon efficiency (%)	91.07	91.30	−0.25 %
FT production (t/h)	46.2	46.4	−0.43 %
FT reactor volume (m^3)	403.6	645	−37 %
Required power SOEC (MW)	423	415	1.8 %
CO_2 released (kg/l)	0.246	0.240	2.6 %
Steam to SOEC (t/h)	138	137	0.46 %
Recycle flow to gasifier (t/h)	19.2	19.5	−1.7 %
Tail gas composition (%)			
H_2	50.3	50.6	−0.6 %
CO	25.4	25.5	−0.6 %
CH_4	13.5	12.7	6.5 %
CO_2	1.8	1.8	0.32 %
N_2	3.3	3.4	−1.6 %
CO_2 molar flow rate (kmol/h)			
Recycle to EFG	23.7	23.6	0.42 %
RWGS feed	488.6	473.2	3.25 %
RWGS outlet	271.6	265.1	2.45 %
Acid gas purge	244.4	238.2	2.60 %

a constant split of 8.8 % of the recycle flow and the recycle flow is lower than in the reference case, these additional emissions must result from AGC. This implies a higher CO_2 content after the RWGS reactor than with Hillestad et al., potentially caused by the different tail gas composition in this study, leading to an increased water content in the RWGS feed, which shifts the equilibrium to a lower CO_2 conversion. Reducing the water content of the biomass by 50 % reduces the CO_2 emissions to 0.231 kg/l, which is 3.9 % lower than in the reference case. Simultaneously, the carbon efficiency increases to 91.51 %, producing about 0.2 t/h of additional fuel and requiring a slightly increased power supply for the SOEC (425 MW instead of 423 MW). Therefore, further research into the effect of removing water before the RWGS reactor could be beneficial in increasing carbon efficiency and lowering specific electricity requirements for fuel production. In conclusion, the model developed in this work is in good agreement with the reference model by Hillestad et al. [3] despite a few deviations, and is therefore considered to be validated.

3.2. Carbon and mass flow analysis

In this section, an analysis of the mass flows in the process cases is undertaken, with a focus on carbon flows as a critical factor in the success of various PBtL processes. Figs. 9 and 10 illustrate the Sankey diagrams of the mass flow rates of the Purge-tF and WGS-adj process configurations, with the remaining process configurations (PBtL, $FAPBtL_{purge}$, and $FAPBtL_{recycle}$) shown in Appendix A, Supplementary Figs. A10–A12. Carbon flows are highlighted in orange, pure water and water flows with negligible contaminants are shown in light blue, oxygen flows are shown in dark blue, and all remaining flows are highlighted in red. Table 8 and Fig. 11 contain key values for the carbon and mass analysis, with the product yield defined as the ratio of the product mass output and the biomass input [5]. The emissions from the use of electricity are calculated using a value of 30 g_{CO_2}/kWh, which was reported by Ember for the year 2023 [57].

The highest carbon efficiency (91.07 %) is achieved in both the PBtL and Purge-tF cases. In comparison, the FAPBtL cases exhibit lower carbon efficiencies: 74.66 % in the purge case and 88.55 % in the recycle case. The WGS-adj cases cover a carbon efficiency range from 67.09 % ($WGS\text{-}adj_{max}$, which is the high steam injection edge case, where the WGS equilibrium is shifted towards CO_2 production until the oxygen requirement in the EFG is just met by the SOECs, as shown in Fig. 10) to 91.07 %, which corresponds to the other edge case (*i.e.*, the PBtL process). Consequently, since the biomass inlet flow is equal in all cases, the highest FT production rates are also found in the PBtL and Purge-tF cases, with production rates exceeding 46 t/h. Carbon losses can occur in three main locations: AGC, purging *via* steam production, and purging *via* the FASOEC anodes. In all cases except for the $FAPBtL_{purge}$ case, the highest carbon losses occur in the AGC unit, making it a crucial sub-process for achieving higher carbon efficiencies. As suggested in the literature [7,8], recycling a portion of the acid gas to the RWGS reactor could boost fuel production. However, this recycling would also increase the need for AGC, thus raising process costs. In the $FAPBtL_{purge}$ case, most CO_2 is lost *via* the FASOECs, since this is the only case where the entire FT tail gas is purged instead of recycled. Consequently, with no carbon recycled to the EFG, the losses in the AGC unit are slightly reduced compared to the PBtL case. In the $WGS\text{-}adj_{max}$ case, substantial carbon losses occur in the AGC unit due to the high conversion of CO to CO_2 in the WGS reactor. The specific emissions are highest in the $WGS\text{-}adj_{max}$, $WGS\text{-}adj_{purge}$, and $FAPBtL_{purge}$ cases, which have the lowest carbon efficiencies, resulting in more carbon being lost as CO_2 emissions, as shown in Fig. 11. It should be noted that the actual emissions from the FASOECs are higher than in the calculation, as the utilization of hydrocarbons with chain lengths of two or more in the FASOECs has not been considered in this work. In practice, these components will also be used by the FASOECs, leading to additional CO_2 emissions. For instance, the specific emissions in the Purge-tF case should match those in the PBtL case, as both result from the same purge stream, yet the specific emissions of the Purge-tF process are 4.8 % lower in comparison to the PBtL case. However, accounting for the utilization of hydrocarbons with chain lengths of two or more in the FASOEC model would also offer additional reductions in electrical energy demands, thus improving the performance and feasibility of the Purge-tF process while retaining the same carbon efficiency as the PBtL process configuration.

Other important factors to consider are water consumption, as water availability can be limited in certain regions, and the surplus oxygen produced by the electrolysis cells that can be sold for profit. In the case of the former, the water consumption rate ranges from 126 t/h in the $FAPBtL_{purge}$ case to 162 t/h in the $FAPBtL_{recycle}$ case, as shown in Table 8. This variation is due to the absence of FT tail gas recycling in the former and the increased hydrogen requirement in the latter case. Most processes produce more water than they consume, apart from some WGS-adj cases. This is partly due to the water content of the biomass (4.2 t/h, not considered in the water usage), but also indicates that dry biomass contains more hydrogen than the amount that ends up in the produced hydrocarbons in these cases. Theoretically, it would be possible to run the process without the need for external water input. However, it would be necessary to investigate whether the electrolysis cells can handle potential impurities in the waste water streams from the separation unit of the FT reactors. For surplus oxygen production, it is shown in Table 8 that the PBtL and Purge-tF processes generate the most oxygen, thus offsetting a significant amount of the production costs for the FT fuel, while the $WGS\text{-}adj_{max}$ process configuration generates no surplus oxygen since it is designed to match the oxygen demands of the EFG.

In summary, the PBtL and Purge-tF cases represent the most favorable options regarding carbon efficiency, FT production, and specific CO_2 emissions, while the $WGS\text{-}adj_{max}$ and $WGS\text{-}adj_{purge}$ process configurations generate the most CO_2 emissions, as shown in Fig. 11.

3.3. Energy analysis

Another critical factor in the feasibility of PBtL processes is energy utilization. This analysis considers heat streams, the electricity required by the electrolysis cells, and the energy contained in the mass flows. However, the energy demand for the auxiliary units such as those for pumps and compressors is neglected. The energy for the auxiliaries is strongly dependent on process design factors, such as pipe sizes, which do not depend on the technologies being used. For better comparability

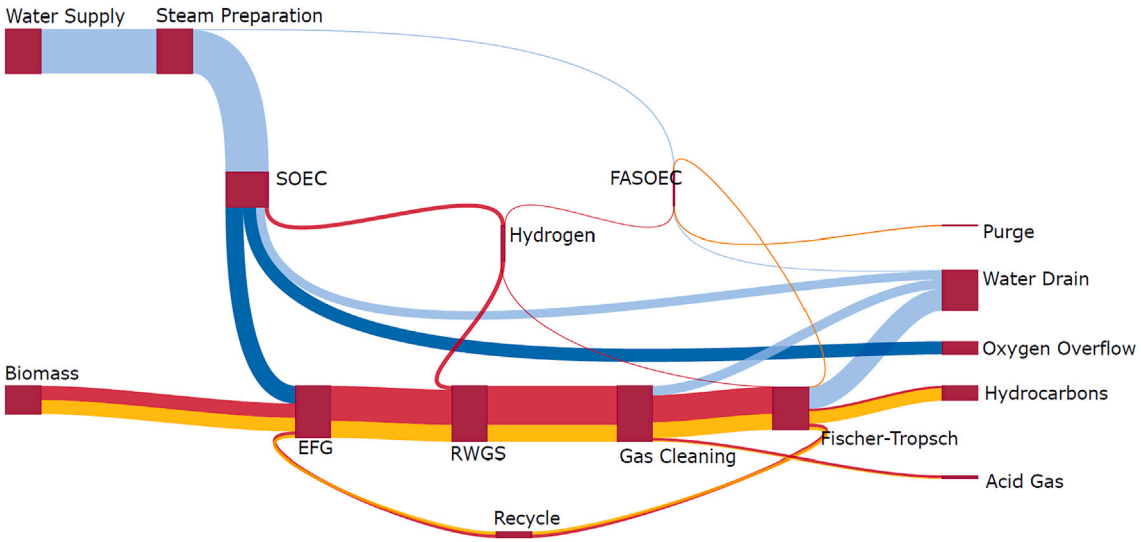

Fig. 9. Sankey chart of the mass flows in the Purge-tF case. Carbon flows are shown in orange, pure water flows and water flows with negligible amounts of contaminants in light blue, oxygen flows in dark blue, and all other flows are shown in red. Block inlets are on the left/top, outlets on the right/bottom, apart from the recycle, where the outlet is on the left and the inlet is on the right. (For interpretation of the references to colour in this figure legend, the reader is referred to the web version of this article.)

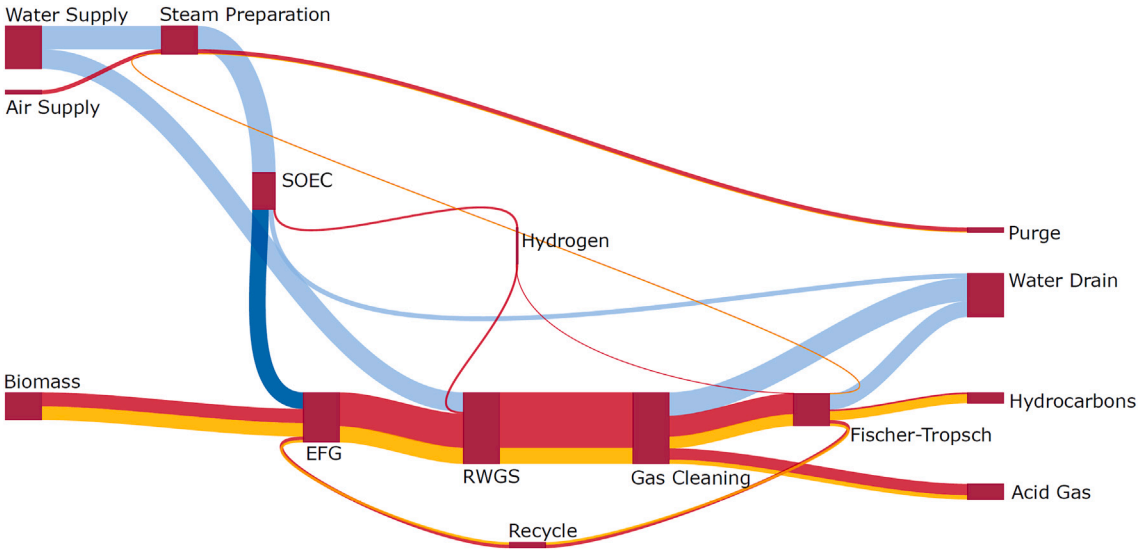

Fig. 10. Sankey chart of the mass flows in the WGS-adj$_{max}$ case for 100 % hydrogen bypass and an injection of 61,500 kg/h of steam in the (R)WGS reactor (the SOEC enough oxygen to satisfy the EFG demand without having any surplus). The same notation for orange, light blue, dark blue, and red lines as in Fig. 9 is used. (For interpretation of the references to colour in this figure legend, the reader is referred to the web version of this article.)

with other PBtL processes, such energy contribution has been neglected in this work. To calculate the energy contained in the mass flows, a reference point is considered (see Section 2.2.10 for more details).

The resulting Sankey diagrams for energy flows of each process case are shown in Figs. 12 and 13 (Purge-tF and WGS-adj$_{max}$, respectively) and Appendix A, Supplementary Figs. A13–A15 (PBtL, FAPBtL$_{purge}$, and FAPBtL$_{recycle}$), with energy percentages based on the energy content of the biomass inlet stream. Table 9 contains key values for the energy analysis, including the electrification rate, which is defined as ratio between the electric energy and the energy contained in the biomass, and the energy yield, which is defined as the ratio of the energy in the product and the sum of the electric energy and the energy contained in the biomass [5]. As shown in the Sankey diagrams and Table 9, the WGS-adj$_{max}$ case exhibits the lowest electricity consumption in the electrolysis cells (6.635 kWh/kg$_{Fuel}$), as well as the fewest number of employed electrolysis cells. Conversely, the PBtL case has the highest specific power requirement of 9.176 kWh/kg$_{Fuel}$. However, this coincides with the highest hydrocarbon production rate (see Section 3.2), while the WGS-adj$_{max}$ process configuration has a specific CO_2 emission rate that is nearly three-times higher than the PBtL case (see Fig. 11). The FAPBtL$_{recycle}$ case requires the highest number of electrolysis cells, which is due to the conversion of high-energy components, such as CO, H_2, and CH_4, into CO_2 and H_2O in the FASOEC anode, where the CO_2 needs to be reconverted into CO in the RWGS reactor using additional hydrogen, which necessitates a higher specific electrolysis energy demand.

An additional finding from the energy analysis is that there exists an optimal fuel utilization value in the FASOEC's anode that minimizes the specific electrolysis energy demand per mass of FT fuel produced in the FAPBtL$_{purge}$ and FAPBtL$_{recycle}$ process configurations. Fig. 14(a) illustrates these minima, where the optimum FASOEC fuel utilization

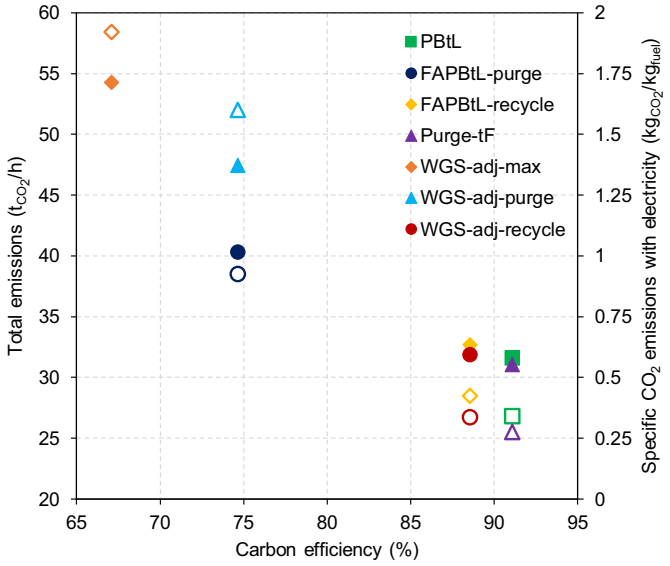

Fig. 11. Total CO_2 emissions (white-filled markers) and specific CO_2 emissions per mass of fuel produced (solid markers) as a function of carbon efficiency for each process configuration. (For interpretation of the references to colour in this figure legend, the reader is referred to the web version of this article.)

value in the $FAPBtL_{recycle}$ case lies at approximately 0.75, while the optimum in the $FAPBtL_{purge}$ case lies at approximately 0.93. These minima are a result of a trade-off between increased energy exploitation of the supplied fuel with increasing fuel utilization in the anode and an increased operating potential due to increasing concentration polarization in the cells. It is important to note that mitigating the rate of carbon deposition in the FASOEC's anode, which can otherwise lead to catalyst deactivation and cell failure, requires operating the cell at increased current densities and fuel utilization values that approach unity [29,58–61]. This highlights an additional trade-off between extending the longevity of FASOECs and reducing the specific electrolysis energy demand per mass of FT fuel, but is beyond the scope of the current study. These variations in specific electrolysis energy demand per mass of FT fuel produced are shown in Fig. 14(b) as a function of the carbon efficiency for each of the process configurations. The minimum specific electrolysis energy demand for the $FAPBtL_{purge}$ process configuration shown in Fig. 14(b) corresponds to a fuel utilization value in the FASOEC of 0.93, while the minimum demand for the $FAPBtL_{recycle}$ process case is attained with a fuel utilization factor of approximately 0.75. It is also shown in Fig. 14(b) that the variations in the WGS-adj process cases have an advantage over both FAPBtL cases, as the former require less specific electrolysis energy than the FAPBtL cases at the same carbon efficiency and FT fuel production rate. However, these reductions in specific electrolysis energy demands occur at the expense of an increase in specific CO_2 emissions, as illustrated in Fig. 11. Additionally, the Purge-tF process configuration requires slightly less electrical energy than the PBtL case at the same carbon efficiency. In Fig. 14(c), the number of electrolysis cells required by each process configuration is also evaluated as a function of process carbon efficiency. Similar to the previous comparison, the WGS-adj cases have an advantage over the FAPBtL cases, since the WGS-adj cases require less electrolysis cells while having the same carbon efficiency. Moreover, it is interesting to note that the PBtL and Purge-tF cases require the same number of electrolysis cells.

3.4. Heat integration

As evident from the Sankey diagrams in Figs. 12 and 13 and Appendix A, Supplementary Figs. A13–A15, cooling flow rates exceed heating flow rates in all considered process cases. To investigate whether the heating demands of the endothermic process units can be satisfied without the need for external energy sources, heat integration is performed. It is assumed that the material streams can be cooled by releasing heat to the environment at 20 °C, and the minimum temperature difference in the heat exchangers is 20 °C. The resulting composite curves for the Purge-tF and $WGS\text{-}adj_{max}$ cases can be found in Fig. 15 (a detailed description on the composite curves can be found in [62]).

The pinch in heat integration is the point where the heat integration system is most constrained – heat should not flow over the pinch point. Therefore, external heating is required for temperatures above the pinch, while external cooling is necessary below the pinch. In all considered cases, no external heating is required since the pinch point is located at the highest temperature (corresponding to the (R)WGS reactor outlet). Assuming that the cooling of this stream can be achieved using a dry heat exchanger, sufficient heat at an adequate temperature can be recovered from the hot streams to meet the heating demand of the cold streams. As described in Section 2.2.1, 18.5 MW of heat would be necessary for biomass drying. All considered cases have over 100 MW of heat available at a temperature of 200 °C, thus meeting the heat requirement for biomass drying. All process variants still have significant amounts of heat available, which could be used in district heating systems or converted into electricity in steam or organic Rankine cycles, offering

Table 8
Key values in the carbon and mass analysis. $WGS\text{-}adj_{purge}$ and $WGS\text{-}adj_{recycle}$ have the same carbon efficiencies as $FAPBtL_{purge}$ and $FAPBtL_{recycle}$, respectively, for even comparison between process configurations.

Process configuration	PBtL	$FAPBtL_{purge}$	$FAPBtL_{recycle}$	Purge-tF	$WGS\text{-}adj_{max}$	$WGS\text{-}adj_{purge}$	$WGS\text{-}adj_{recycle}$
Carbon efficiency (%)	91.07	74.66	88.55	91.07	67.09	74.66	88.55
FT Production (t/h)	46.2	37.9	45.0	46.2	34.1	37.9	45.0
Product yield ($kg_{fuel}/kg_{biomass}$)	0.555	0.455	0.540	0.555	0.409	0.455	0.540
Hydrogen requirement (t/h)	12.6	11.5	14.8	12.6	6.7	8.4	11.7
Surplus oxygen (t/h)	43.13	22.62	36.50	40.65	0.00	13.43	38.42
Total emissions (t_{CO_2}/h)	26.8	38.5	28.5	25.5	58.4	52.0	26.7
AGC (t_{CO_2}/h)	10.9	9.4	14.1	10.9	48.9	37.1	15.0
Steam preparation (t_{CO_2}/h)	3.2	0	0	0	2.7	2.9	3.1
FASOECs (t_{CO_2}/h)	0	19.7	2.1	2.1	0	0	0
Electricity (t_{CO_2}/h)	12.7	9.4	12.3	12.5	6.8	12.0	8.6
Specific CO_2 emissions:							
Without electricity (kg_{CO_2}/kg_{fuel})	0.305	0.768	0.360	0.281	1.513	1.055	0.402
With electricity (kg_{CO_2}/kg_{fuel})	0.580	1.016	0.633	0.552	1.713	1.372	0.593
Water usage (t/h)	138	126	162	138	135	127	131
Water drainage (t/h)	152	144	186	154	211	124	118
Net water usage (t/h)	−14	−18	−24	−16	−56	3	13

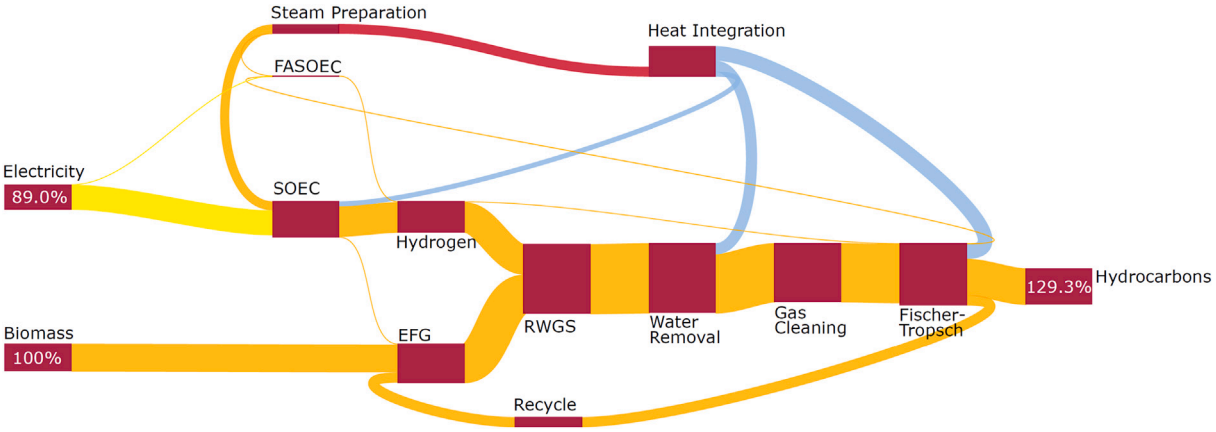

Fig. 12. Sankey chart of the energy flows in the Purge-tF case. Minor heat streams are not shown for the sake of simplicity. Enthalpy streams at the environmental temperature plus the temperature difference in the heat exchangers (*i.e.*, 40 °C) are neglected, due to the negligible energy contained in them and the impossibility of using them for further heat integration. Streams are shown in orange for enthalpy, yellow for electricity, red for heating, and blue for cooling. Inlets for blocks are on the left/top, and outlets are on the right/bottom, apart from the steam preparation, heat integration, and recycle blocks, where the inlet is on the right and the outlet is on the left. (For interpretation of the references to colour in this figure legend, the reader is referred to the web version of this article.)

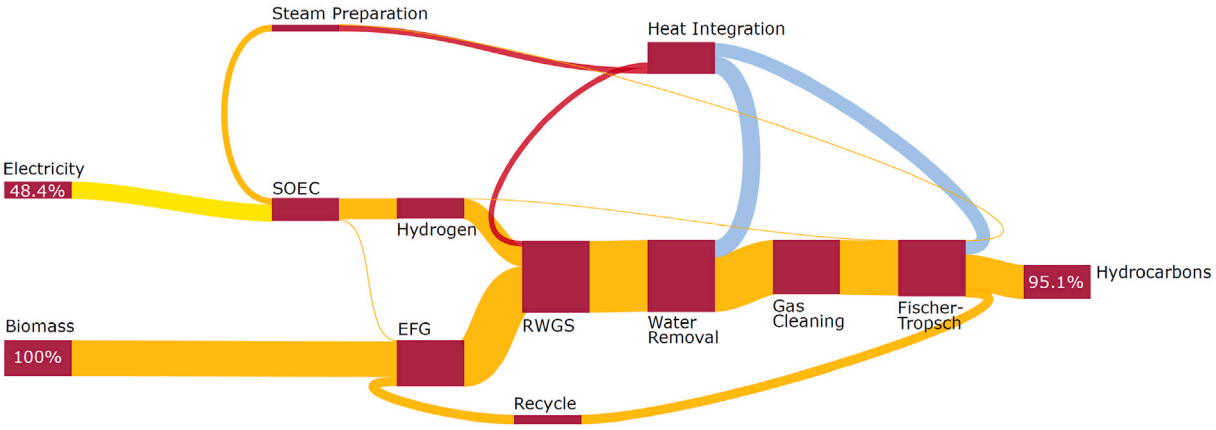

Fig. 13. Sankey chart of the energy flows in the WGS-adj$_{max}$ edge case with maximal steam injection, where the SOECs still provide enough oxygen for the EFG. Minor heat streams are not shown for the sake of simplicity. The same description and notation for orange, yellow, red, and blue lines as in Fig. 12 is used. (For interpretation of the references to colour in this figure legend, the reader is referred to the web version of this article.)

Table 9
Key values in the energy analysis. WGS-adj$_{purge}$ and WGS-adj$_{recycle}$ have the same carbon efficiencies as FAPBtL$_{purge}$ and FAPBtL$_{recycle}$, respectively, as in Table 8, for fair comparison between process configurations.

Process configuration	PBtL	FAPBtL$_{purge}$	FAPBtL$_{recycle}$	Purge-tF	WGS-adj$_{max}$	WGS-adj$_{purge}$	WGS-adj$_{recycle}$
Total electrolysis power requirement (MW)	424	313	409	416	227	287	401
Specific electrolysis energy (kWh/kg$_{fuel}$)	9.176	8.247	9.101	9.002	6.635	7.577	8.921
Number of electrolysis cells (–)	86,700	79,400	102,000	86,700	46,300	58,800	82,100
Electrification Rate (kWh$_{elec}$/kWh$_{biomass}$)	0.975	0.719	0.941	0.957	0.521	0.661	0.922
Energy Yield (kWh$_{fuel}$/kWh$_{elec+biomass}$)	0.703	0.663	0.696	0.710	0.672	0.685	0.703

great potential to further reduce the net electricity demand of the process variants [63,64]. The composite curves for the remaining process configurations are illustrated in Appendix A, Supplementary Fig. A16.

3.5. Economic analysis

Thus far, we have revealed the advantages and disadvantages of each process configuration by comparing energy demands, carbon efficiencies, product yield, and specific CO_2 emissions through mass and energy analyses. WGS-adj processes have demonstrated significant reductions in specific electrolysis energy demands and the number of required electrolysis cells in comparison to Purge-tF, PBtL, and the FAPBtL processes. However, these reductions are attained at the expense of reduced carbon efficiencies and increased specific CO_2 emissions. For instance, if we compare the FAPBtL$_{purge}$ and WGS-adj$_{purge}$ cases with the same carbon efficiency and FT fuel production rate, the former requires 8.1 % more electrical energy per mass of FT fuel produced, while emitting 35 % less CO_2 per mass of FT product. This example presents an economic dilemma: minimizing electricity consumption to mitigate process operating costs can lead to higher carbon tax penalties as a result of increased CO_2 emissions. This presents the need for an economic analysis to evaluate which process configurations are most profitable and

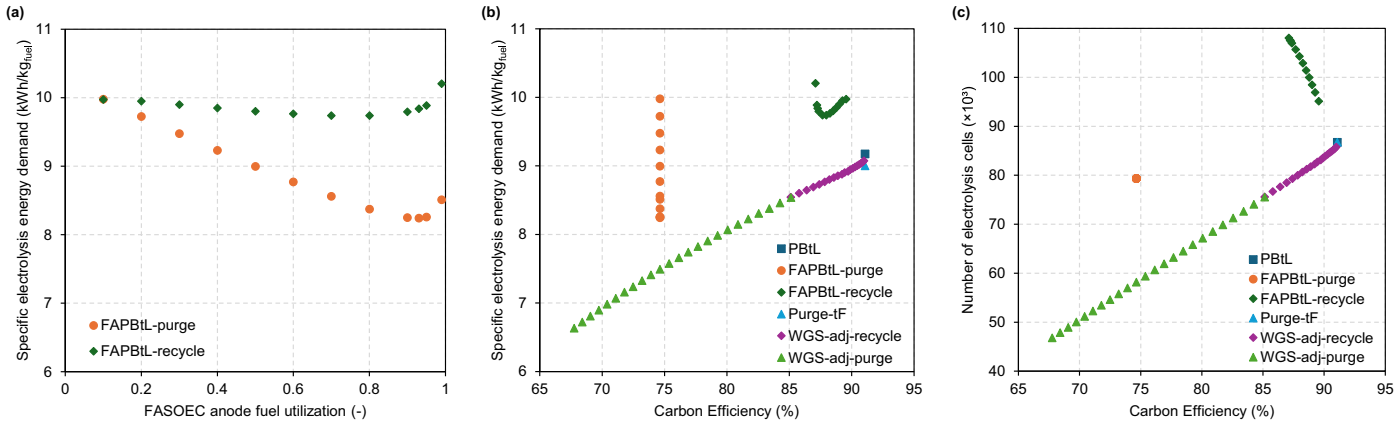

Fig. 14. (a) Specific electrolysis energy for FAPBtL$_{recycle}$ and FAPBtL$_{purge}$ process configurations as a function of fuel utilization in the FASOEC anode; (b) comparison of the specific electrolysis energy demands as a function of carbon efficiency across all process configurations; and (c) comparison of the required number of electrolysis cells to meet process hydrogen demands versus carbon efficiency for each process configuration. The leftmost green triangle for the WGS-adj$_{purge}$ process corresponds to the WGS-adj$_{max}$ configuration. (For interpretation of the references to colour in this figure legend, the reader is referred to the web version of this article.)

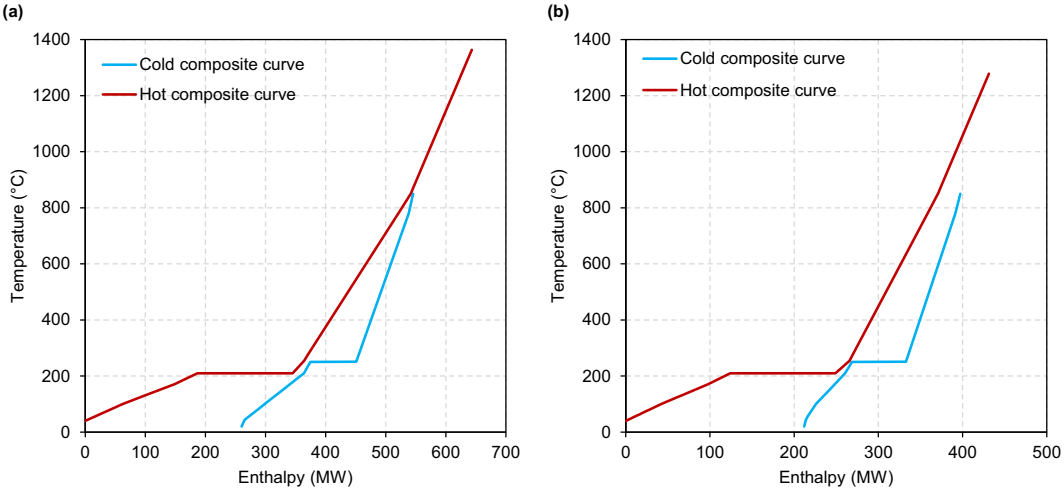

Fig. 15. Composite curves for the (a) Purge-tF and (b) WGS-adj$_{max}$ process configurations.

elucidate whether operating costs and carbon tax penalties offset one another.

Fig. 16 illustrates the NPC for the different process configurations, Table 10 summarizes the raw materials and utility costs of the Purge-tF process configuration, and Supplementary Table A2-A14 list the equipment costs and raw materials and utility costs of the remaining process configurations. The information provided in these tables is used to evaluate the NPC value for each process variant using TEPET. The largest contributors to the NPC across all process configurations are the cost of electricity, biomass (dried), SOEC stack replacement, EFG, and FT synthesis unit. The WGS-adj$_{max}$ and WGS-adj$_{purge}$ generate the highest carbon tax penalties as a result of their reduced carbon efficiencies, as discussed above. However, despite these carbon tax penalties, these processes have the lowest NPC values in comparison to the remaining processes, since they have lower specific electrolysis energy demands (*i.e.*, lower electricity demands) and require fewer SOECs to produce the hydrogen needed for their respective processes. As a result of having the lowest NPC value of 2.66 €$_{2023}$/kg$_{fuel}$, the WGS-adj$_{max}$ process represents the most economically competitive configuration, which comes at the expense of a significantly lower carbon efficiency compared to the other processes, but offers improved flexibility with fluctuating electricity prices by adjusting carbon efficiency. Conversely, the FAPBtL$_{recycle}$ process configuration produces the highest NPC value of 3.22 €$_{2023}$/kg$_{fuel}$, as it requires the highest number of SOECs and has the highest specific electrolysis energy demand. This is a result of the additional amount of hydrogen that is needed to convert the CO_2 from the FASOEC tail gas into the desired products for the FT reactor inlet. Accordingly, the FAPBtL$_{recycle}$ process concept represents the least competitive option from both technical and economic perspectives.

A sensitivity analysis was performed for all process configurations to evaluate the influence of parameter variation on NPC. Supplementary Fig. A17 illustrates the NPC of the WGS-adj$_{max}$ process configuration versus the percentage of parameter variation, which includes the cost of electricity, interest rate, SOEC investment and stack replacement costs, and carbon taxation (*i.e.*, the most influential parameters that govern NPC for the process configurations investigated in this study). It should be noted that the sensitivity analysis of the remaining process configurations yields similar results to the WGS-adj$_{max}$ case. Assuming a 50 % reduction in the cost of electricity and a 50 % reduction in SOEC investment and stack replacement costs would result in the same process ranking shown in Fig. 16 with respect to NPC. This means that varying the most influential cost parameters for each process configuration with

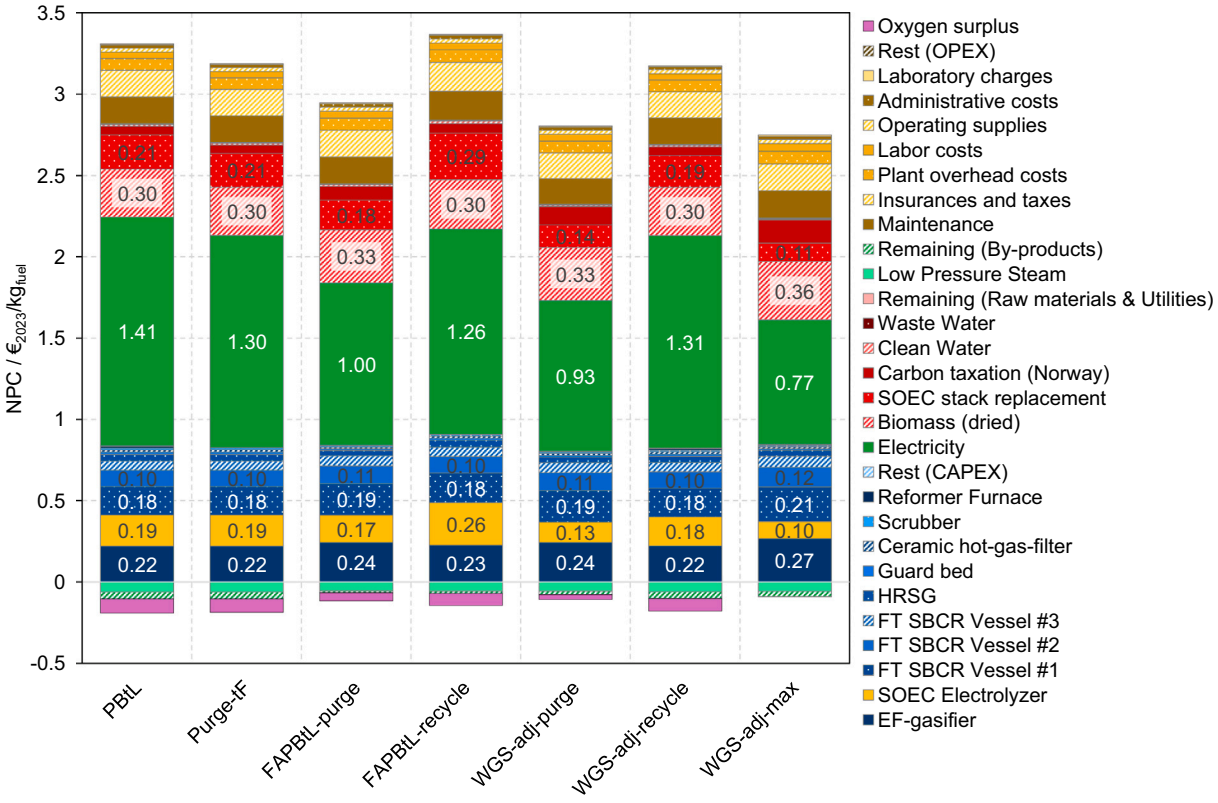

Fig. 16. The net production cost (NPC) of the Fischer–Tropsch fuel for each of the process configurations. In the order from lowest NPC value to highest (*i.e.*, most economically competitive to least), the process variants are: WGS-adj$_{max}$ (2.66 €$_{2023}$/kg$_{fuel}$), WGS-adj$_{purge}$ (2.70 €$_{2023}$/kg$_{fuel}$), FAPBtL$_{purge}$ (2.83 €$_{2023}$/kg$_{fuel}$), Purge-tF (3.00 €$_{2023}$/kg$_{fuel}$), WGS-adj$_{recycle}$ (3.00 €$_{2023}$/kg$_{fuel}$), PBtL (3.12 €$_{2023}$/kg$_{fuel}$), and FAPBtL$_{recycle}$ (3.22 €$_{2023}$/kg$_{fuel}$).

Table 10
Raw material and utility costs used in the techno-economic analysis for the Purge-tF process configuration. M€ corresponds to millions of €.

Raw material/utility	Quantity per hr	Functional unit	Market price (year 2023)	Unit	Total costs per year	Currency	Reference
Electrolysis water	157.33	m^3/h	2.9	€/m^3	3.77	M€	[27]
Cobalt catalyst	2.79	kg/h	32.92	€/kg	0.76	M€	[65]
Cooling water	5,654.09	m^3/h	–	€/m^3	–	M€	[27]
Electricity (grid)	449.13	MWh/h	121.08	€/MWh	449.19	M€	[66]
SOEC replacement	1.99	stack/h	4,384.44	€/stack	71.68	M€	[3]
Selexol	0.0034	t/hr	6,271.19	€/t	0.17	M€	[67]
Waste water	110.97	m^3/h	1.31	€/m^3	1.20	M€	[56]
Wet biomass	87.50	t/h	141.20	€/t	102.05	M€	[68]
Carbon tax (Norway)	25.5	t/h	83.47	€/t	17.58	M€	[69]
Total costs					646.40	M€	–
By-products							
High pressure steam	−53.15	t/h	33.44	€/t	−1468	M€	[70]
Low pressure steam	−86.41	t/h	29.64	€/t	−21.16	M€	[70]
Oxygen surplus	−40.65	t/h	84.63	€/t	−28.42	M€	[71,72]
Total revenue					−64.25	M€	–

respect to NPC by 50 % would still result in the WGS-adj$_{max}$ process configuration being the most competitive among those investigated in this study.

Comparing the NPC value range reported in this study (2.66–3.22 €$_{2023}$/kg$_{fuel}$ (1.94–2.35 €$_{2023}$/l$_{fuel}$)), in tandem with the carbon efficiencies (67.1–91.7 %), demonstrates the cost competitiveness of the developed process configurations in comparison to previous studies. For example, Isaacs et al. [21] reported NPC values of between 2.02 and 4.90 €/l$_{fuel}$ (1.00 € = 1.04 $ USD) for PBtL processes deployed across the United States in the year 2030. Herz et al. [73] developed a Power-to-X (PtX) process model which predicted NPC values of 2.66–3.36 €$_{2022}$/kg$_{fuel}$ by the year 2050 with carbon efficiencies of less than 65 %, while Markowitsch et al. [74] reported a carbon efficiency of 85 % with an NPC value of 8.40 €$_{2022}$/kg$_{fuel}$. Additionally, Pratschner et al. [72] demonstrated that the NPC for the FT fuels can be reduced from 2.42–4.56 €$_{2022}$/kg$_{fuel}$ to 1.28–2.40 €$_{2022}$/kg$_{fuel}$ by switching from a grid-based electricity supply to an off-grid supply, cutting their NPC values by over 50 %. With the cost of electricity being the main contributor to the NPC values in all process configurations developed herein, pursuing off-grid renewable and sustainable power may provide a promising alternative for further reducing NPC values. Doing so can promote the economic feasibility of producing sustainable aviation fuels in order to alleviate dependence on the existing fossil fuel-based infrastructure.

4. Conclusions

In this work, a power- and biomass-to-liquid (PBtL) process model comprising several process configurations has been developed in Aspen HYSYS to integrate fuel-assisted solid oxide electrolysis cells (FASOECs) and adjustments in the water gas shift reactor equilibrium (WGS-adj). The model developed herein has been validated with simulation results from the literature. Furthermore, a techno-economic analysis has been conducted with the aid of TEPET (a techno-economic tool developed by the German Aerospace Center (DLR)) to calculate mass and energy balances and the net production costs (NPC) of each process configuration for the case study of Norway for the year 2023. The key conclusions that can be drawn from this study are as follows:

- The use of Fischer–Tropsch (FT) tail gas as fuel for the FASOECs appears to be disadvantageous in all fuel-assisted PBtL (FAPBtL) process configurations, since the effect of a reduction in the specific electrolysis energy demand per amount of produced hydrogen is surpassed by an increased specific hydrogen demand per produced fuel compared to the respective WGS-adjusted case. The NPC values of the $FAPBtL_{recycle}$ process is the highest among all cases at 3.22 $€_{2023}/kg_{fuel}$.
- Alternatively, the FT tail gas purge stream can be used as fuel in the FASOECs (the Purge-tF case), thereby reducing the specific electrolysis energy demands of the process and its NPC value. The Purge-tF process yields the highest carbon efficiency while requiring less electricity than the conventional PBtL process, resulting in NPC values of 3.00 $€_{2023}/kg_{fuel}$ and 3.12 $€_{2023}/kg_{fuel}$ for the Purge-tF and PBtL processes, respectively.
- The adjustment of the water gas shift equilibrium *via* hydrogen bypass and steam addition can be used to reduce hydrogen demands and the specific electrolysis energy of the process (the WGS-adj process variants). However, this comes at the expense of a reduced fuel production rate and consequently carbon efficiency. For the same carbon efficiency and fuel production, the WGS-adj processes have lower specific electrolysis energy requirements and lower NPC values than the FAPBtL process variants.
- In order from the lowest to the highest NPC value (*i.e.*, most economically competitive to least), the process variants are: $WGS\text{-}adj_{max}$ (2.66 $€_{2023}/kg_{fuel}$), $WGS\text{-}adj_{purge}$ (2.70 $€_{2023}/kg_{fuel}$), $FAPBtL_{purge}$ (2.83 $€_{2023}/kg_{fuel}$), Purge-tF (3.00 $€_{2023}/kg_{fuel}$), $WGS\text{-}adj_{recycle}$ (3.00 $€_{2023}/kg_{fuel}$), PBtL (3.12 $€_{2023}/kg_{fuel}$), and $FAPBtL_{recycle}$ (3.22 $€_{2023}/kg_{fuel}$).
- The heat integration analysis of all process configurations has proven that sufficient heat can be recovered within the processes to meet the heating demands, and no external heat sources are required. Additionally, the burning of the FT tail gas purge stream is not required for additional heat production. The excess heat (at least part of it) can be used to preheat the feed stream to the entrained flow gasifier (EFG). Providing thermal energy to the gasifier will reduce the hydrogen demand, as less oxidizing agent is needed to achieve the operating temperature of the gasifier, thus improving the syngas quality [75].
- The SOECs, EFG, and FT reactors are the main contributors to the equipment costs, while electricity, SOEC stack replacement, and the cost of biomass are the key contributors to the operating costs.

While this work has evaluated the use of FASOECs and the integration of WGS-adj systems in PBtL processes, further work is required to improve their competitiveness. For instance:

- An investigation should be undertaken to evaluate the optimal WGS equilibrium as a function of the electricity price – high electricity prices might require a lower specific electrolysis energy for optimal economic performance.
- All processes, with the exception of WGS-adj process configurations, produce more water than they require in the SOECs. An investigation into whether the quality of the produced water is sufficient for the electrolysis could be undertaken, or whether a water purification system would be technically and economically feasible.
- All process cases exhibit a high heat excess at medium to high temperatures. Heat recovery and conversion processes should be investigated as a way to reduce the net electricity demand of the processes.
- The considered EFG outlet temperature is very high (*i.e.*, 1600 °C) in the reference process to promote carbon conversion. However, such high operating temperatures require expensive materials for the gasifier to resist the thermal stress. Therefore, investigating how reducing the EFG outlet temperature affects the key performance indicators could be worthwhile.
- While operating temperatures of 850 °C is standard for SOECs and FASOECs [48], their operating pressures have been limited to 25 bar in previous experiments [76], which is less than the value used in this study (40 bar). Therefore, experimental validation is required. However, with projected material advancements in SOEC technologies, it is expected that these systems will be able to operate at even higher pressures in the foreseeable future [48].
- The FASOEC model used in this study considers the use of CO, H_2 and CH_4; however, a small amount (<1 % mol) of higher hydrocarbons are present in the FT tail gas. A FASOEC model including the use of higher hydrocarbons should be developed to evaluate the impact of considering higher hydrocarbons in the FASOEC on the key process performance indicators. It should be noted, however, that the use of bio-ethanol as alternative anodic fuel has been demonstrated experimentally by Liu et al. [52] in FASOECs for the production of hydrogen, where they demonstrated improved voltage stability at current densities of higher than 3.0 A cm^{-2}. This highlights the versatility of FASOECs in their ability to use an assortment of fuel mixtures to reduce the energy demands of hydrogen production.
- The Purge-tF process case has been identified as a competitive process configuration in this study due to its high carbon efficiency. However, the ratio of the FT tail gas that is purged has been set to a fixed value (8.8 %). An investigation could be undertaken to determine the optimal purge ratio for the Purge-tF process – a higher purge ratio would be beneficial for reducing the electricity requirement and the sizing of the process, but it would also reduce fuel production and carbon efficiency.
- Carbon deposition in FASOECs is an important concern that influences their longevity. Strategies including increasing current density and fuel utilization can mitigate carbon deposition, as demonstrated by the FASOEC model used in the current study [29] and other experimental studies [58–61]. An additional study could include investigating the optimum trade-off between minimizing carbon deposition to extend FASOEC operating life while reducing the specific electrolysis energy demand per mass of FT fuel.
- An investigation of the acid gas cleaning (AGC) sub-process, which is responsible for the highest carbon loss in all process configurations (~75 % in most cases), should be undertaken to reduce the carbon losses in the system. Possibilities would include recycling most of the acid gases removed in the AGC to the RWGS reactor, or researching a process less selective towards CO_2.

CRediT authorship contribution statement

Samuel M. Kämer: Conceptualization, methodology, software, validation, formal analysis, investigation, visualization, writing – original draft, writing – review & editing. **Anders S. Nielsen**: Conceptualization, software, visualization, writing – original draft, writing – review & editing, supervision, and funding acquisition. **Simon Maier**: Methodology, software, formal analysis, visualization, and writing – review & editing. **Simone Mucci**: Conceptualization, writing – review & editing, and supervision. **Magne Hillestad**: Conceptualization, software, writing – review & editing, and supervision. **Odne S. Burheim**: Conceptualization,

visualization, writing – review & editing, supervision, and funding acquisition.

Declaration of generative AI and AI-assisted technologies in the writing process.

During the preparation of this work the author(s) used ChatGPT in order to improve the readability and language of the manuscript. After using this tool/service, the author(s) reviewed and edited the content as needed and take(s) full responsibility for the content of the published article.

Declaration of competing interest

The authors declare that they have no known competing financial interests or personal relationships that could have appeared to influence the work reported in this paper.

Acknowledgments

A.S. Nielsen gratefully acknowledges the funding support from a Natural Sciences and Engineering Research Council of Canada (NSERC) Postdoctoral Fellowship (PDF).

Supplementary data

Supplementary data to this article can be found online at doi:10.1016/j.fuel.2025.135290.

Data availability

Data will be made available on request.

References

[1] Dhakal S, Minx JC, Toth FL, Abdel-Aziz A, Figueroa Meza MJ, Hubacek K, et al. Emissions trends and drivers. In: Intergovernmental panel on climate change (ed.), climate change 2022 - mitigation of climate change. Cambridge, UK and New York, NY, USA: Cambridge University Press; 2022. p. 215–94. doi:https://doi.org/10.1017/9781009157926.004.

[2] Adu-Gyamfi BA, Good C. Electric aviation: a review of concepts and enabling technologies. Transp Eng 2022;9:100134. doi:https://doi.org/10.1016/j.treng.2022.100134.

[3] Hillestad M, Ostadi M, Alamo Serrano G, Rytter E, Austbø B, Pharoah JG, et al. Improving carbon efficiency and profitability of the biomass to liquid process with hydrogen from renewable power. Fuel 2018;234:1431–51. doi:https://doi.org/10.1016/j.fuel.2018.08.004.

[4] Schmidt P, Batteiger V, Roth A, Weindorf W, Raksha T. Power-to-liquids as renewable fuel option for aviation: a review. Chem Ing Tech 2018;90:127–40. doi:https://doi.org/10.1002/cite.201700129.

[5] Dossow M, Klüh D, Umeki K, Gaderer M, Spliethoff H, Fendt S. Electrification of gasification-based biomass-to-x processes – a critical review and in-depth assessment. Energy Environ Sci 2024;17:925–73. doi:https://doi.org/10.1039/D3EE02876C.

[6] Assen NVD, Müller LJ, Steingrube A, Voll P, Bardow A. Selecting CO_2 sources for CO_2 utilization by environmental-merit-order curves. Environ Sci Technol 2016;50:1093–101. doi:https://doi.org/10.1021/acs.est.5b03474.

[7] Dossow M, Dieterich V, Hanel A, Spliethoff H, Fendt S. Improving carbon efficiency for an advanced biomass-to-liquid process using hydrogen and oxygen from electrolysis. Renew Sustain Energy Rev 2021;152:111670. doi:https://doi.org/10.1016/j.rser.2021.111670.

[8] Habermeyer F, Weyand J, Maier S, Kurkela E, Dietrich R-U. Power biomass to liquid — an option for Europe's sustainable and independent aviation fuel production. Biomass Convers Biorefin 2023; doi:https://doi.org/10.1007/s13399-022-03671-y.

[9] Mucci S, Mitsos A, Bongartz D. Combustion versus gasification in power- and biomass-to-X processes: an exergetic analysis. ACS Omega 2024;9:48213–31. doi:https://doi.org/10.1021/acsomega.4c05549.

[10] Hillestad M. Modeling the Fischer–Tropsch product distribution and model implementation. Chem Prod Process Model 2015;10:147–59. doi:https://doi.org/10.1515/cppm-2014-0031.

[11] Houben MP, de Lange HC, van Steenhoven AA. Tar reduction through partial combustion of fuel gas. Fuel 2005;84:817–24. doi:https://doi.org/10.1016/j.fuel.2004.12.013.

[12] Baliban RC, Elia JA, Floudas CA. Toward novel hybrid biomass, coal, and natural gas processes for satisfying current transportation fuel demands, 1: Process alternatives, gasification modeling, process simulation, and economic analysis. Ind Eng Chem Res 2010;49:7343–70. doi:https://doi.org/10.1021/ie100063y.

[13] Kurkela E, Kurkela M, Frilund C, Hiltunen I, Rollins B, Steele A. Flexible hybrid process for combined production of heat, power and renewable feedstock for refineries. Johnson Matthey Technol Rev 2021;65:333–45. doi:https://doi.org/10.1595/205651321X16013744201583.

[14] Ahmad W, Lin L, Strand M. Benzene conversion using a partial combustion approach in a packed bed reactor. Energy 2022;239:122251. doi:https://doi.org/10.1016/j.energy.2021.122251.

[15] Mucci S, Goldstein DP, Bongartz D, Mitsos A. Exergo-techno-economic comparison of power&biomass-to-kerosene pathways. Comput Aided Chem Eng 2024;53:2131–36. doi:https://doi.org/10.1016/B978-0-443-28824-1.50356-2.

[16] Seiler J-M, Hohwiller C, Imbach J, Luciani J-F. Technical and economical evaluation of enhanced biomass to liquid fuel processes. Energy 2010;35:3587–92. doi:https://doi.org/10.1016/j.energy.2010.04.048.

[17] Bernical Q, Joulia X, Noirot-Le Borgne I, Floquet P, Baurens P, Boissonnet G. Sustainability assessment of an integrated high temperature steam electrolysis-enhanced biomass to liquid fuel process. Ind Eng Chem Res 2013;52:7189–95. doi:https://doi.org/10.1021/ie302490y.

[18] Pandey U, Putta KR, Rout KR, Rytter E, Blekkan EA, Hillestad M. Conceptual design and techno-economic analysis of biomass to liquid processes. Front Energy Res 2022;10. doi:https://doi.org/10.3389/fenrg.2022.993376.

[19] Müller S, Groß P, Rauch R, Zweiler R, Aichernig C, Fuchs M, et al. Production of diesel from biomass and wind power – energy storage by the use of the Fischer-Tropsch process. Biomass Convers Biorefin 2018;8:275–82. doi:https://doi.org/10.1007/s13399-017-0287-1.

[20] Gruber H, Groß P, Rauch R, Reichhold A, Zweiler R, Aichernig C, et al. Fischer-Tropsch products from biomass-derived syngas and renewable hydrogen. Biomass Convers Biorefin 2021;11:2281–92. doi:https://doi.org/10.1007/s13399-019-00459-5.

[21] Isaacs SA, Staples MD, Allroggen F, Mallapragada DS, Falter CP, Barrett SRH. Environmental and economic performance of hybrid power-to-liquid and biomass-to-liquid fuel production in the United States. Env Sci Technol 2021;55:8247–57. doi:https://doi.org/10.1021/acs.est.0c07674.

[22] Umweltbundesamt. CO_2-Emissionen pro Kilowattstunde Strom stiegen in 2022; 2023. https://www.umweltbundesamt.de/themen/co2-emissionen-pro-kilowattstunde-strom-stiegen-in.

[23] Intergovernmental Panel on Climate Change, Ed. Annex III: technology-specific cost and performance parameters. Cambridge, UK and New York, NY, USA: Cambridge University Press; 2014.

[24] Habermeyer F, Kurkela E, Maier S, Dietrich R-U. Techno-economic analysis of a flexible process concept for the production of transport fuels and heat from biomass and renewable electricity. Front Energy Res 2021;9:267. doi:https://doi.org/10.3389/fenrg.2021.723774.

[25] Bernical Q, Joulia X, Noirot-Le Borgne I, Floquet P, Baurens P, Boissonnet G. Integrated design of high temperature steam electrolysis and biomass to liquid fuel process. In: 11th International symposium on process systems engineering, volume 31 of computer aided chemical engineering. Elsevier; 2012. p. 865–69. doi:https://doi.org/10.1016/B978-0-444-59506-5.50004-3.

[26] Zhang H, Desideri U. Techno-economic optimization of power-to-methanol with co-electrolysis of CO_2 and H_2O in solid-oxide electrolyzers. Energy 2020;199:117498. doi:https://doi.org/10.1016/j.energy.2020.117498.

[27] Albrecht FG, König DH, Baucks N, Dietrich R-U. A standardized methodology for the techno-economic evaluation of alternative fuels – a case study. Fuel 2017;194:511–26. doi:https://doi.org/10.1016/j.fuel.2016.12.003.

[28] Nielsen AS, Ostadi M, Austbø B, Hillestad M, Del Alamo G, Burheim O. Enhancing the efficiency of power- and biomass-to-liquid fuel processes using fuel-assisted solid oxide electrolysis cells. Fuel 2022;321:123987. doi:https://doi.org/10.1016/j.fuel.2022.123987.

[29] Nielsen AS, Peppley BA, Burheim OS. Tuning transport mechanisms in fuel-assisted solid oxide electrolysis cells for enhanced performance and product selectivity: thermodynamic and kinetic modeling. Chem Eng J 2023;452:139079. doi:https://doi.org/10.1016/j.cej.2022.139079.

[30] Lei L, Wang Y, Fang S, Ren C, Liu T, Chen F. Efficient syngas generation for electricity storage through carbon gasification assisted solid oxide co-electrolysis. Appl Energy 2016;173:52–58. doi:https://doi.org/10.1016/j.apenergy.2016.03.116.

[31] Martinez-Frias J, Pham A-Q, Aceves SM. A natural gas-assisted steam electrolyzer for high-efficiency production of hydrogen. Int J Hydrogen Energy 2003;28:483–90. doi:https://doi.org/10.1016/S0360-3199(02)00135-0.

[32] Wang Y, Liu T, Fang S, Xiao G, Wang H, Chen F. A novel clean and effective syngas production system based on partial oxidation of methane assisted solid oxide co-electrolysis process. J Power Sources 2015;277:261–67. doi:https://doi.org/10.1016/j.jpowsour.2014.11.092.

[33] Tao G, Butler B, Virkar A. Hydrogen and power by fuel-assisted electrolysis using solid oxide fuel cells. ECS Trans 2011;35:2929. doi:https://doi.org/10.1149/1.3570292.

[34] Kyriakou V, Neagu D, Zafeiropoulos G, Sharma RK, Tang C, Kousi K, et al. Symmetrical exsolution of Rh nanoparticles in solid oxide cells for efficient syngas production from greenhouse gases. ACS Catal 2020;10:1278–88. doi:https://doi.org/10.1021/acscatal.9b04424.

[35] Liu T, Liu H, Zhang X, Lei L, Zhang Y, Yuan Z, et al. A robust solid oxide electrolyzer for highly efficient electrochemical reforming of methane and steam. J Mater Chem A 2019;7:13550–58. doi:https://doi.org/10.1039/C9TA00467J.

[36] Patcharavorachot Y, Thongdee S, Saebea D, Authayanun S, Arpornwichanop A. Performance comparison of solid oxide steam electrolysis cells with/without the addition of methane. Energy Convers Manag 2016;120:274–86. doi:https://doi.org/10.1016/j.enconman.2016.04.100.

[37] Luo Y, Shi Y, Li W, Ni M, Cai N. Elementary reaction modeling and experimental characterization of solid oxide fuel-assisted steam electrolysis cells. Int J Hydrogen Energy 2014;39:10359–73. doi:https://doi.org/10.1016/j.ijhydene.2014.05.018.
[38] Phanphanich M, Mani S. Impact of torrefaction on the grindability and fuel characteristics of forest biomass. Bioresour Technol 2011;102:1246–53. doi:https://doi.org/10.1016/j.biortech.2010.08.028.
[39] Arias B, Pevida C, Fermoso J, Plaza M, Rubiera F, Pis J. Influence of torrefaction on the grindability and reactivity of woody biomass. Fuel Process Technol 2008;89:169–75. doi:https://doi.org/10.1016/j.fuproc.2007.09.002.
[40] Wang L, Barta-Rajnai E, Skreiberg Ø, Khalil R, Czégény Z, Jakab E, et al. Impact of torrefaction on woody biomass properties. Energy Procedia 2017;105:1149–54. doi:https://doi.org/10.1016/j.egypro.2017.03.486.
[41] Qin K, Jensen PA, Lin W, Jensen AD. Biomass gasification behavior in an entrained flow reactor: gas product distribution and soot formation. Energy Fuels 2012;26:5992–6002. doi:https://doi.org/10.1021/ef300960x.
[42] Zhou J, Chen Q, Zhao H, Cao X, Mei Q, Luo Z, et al. Biomass–oxygen gasification in a high-temperature entrained-flow gasifier. Biotechnol Adv 2009;27:606–11. doi:https://doi.org/10.1016/j.biotechadv.2009.04.011.
[43] Ostadi M, Rytter E, Hillestad M. Boosting carbon efficiency of the biomass to liquid process with hydrogen from power: the effect of H_2/CO ratio to the Fischer-Tropsch reactors on the production and power consumption. Biomass Bioenergy 2019;127:105282. doi:https://doi.org/10.1016/j.biombioe.2019.105282.
[44] Todic B, Ma W, Jacobs G, Davis BH, Bukur DB. Effect of process conditions on the product distribution of Fischer–Tropsch synthesis over a re-promoted cobalt-alumina catalyst using a stirred tank slurry reactor. J Catal 2014;311:325–38. doi:https://doi.org/10.1016/j.jcat.2013.12.009.
[45] Agazzi B. Design, modeling and comparison of two innovative power-biomass-to-liquid processes [Master thesis]. Milano: Politecnico Milano; 2021.
[46] Demirbas A, Ak N, Aslan A, Sen N. Calculation of higher heating values of hydrocarbon compounds and fatty acids. Pet Sci Technol 2018;36:712–17. doi:https://doi.org/10.1080/10916466.2018.1443126.
[47] Panzone C, Philippe R, Chappaz A, Fongarland P, Bengaouer A. Power-to-liquid catalytic co2 valorization into fuels and chemicals: focus on the fischer-tropsch route. J CO2 Util 2020;38:314–47. doi:https://doi.org/10.1016/j.jcou.2020.02.009.
[48] Chatenet M, Pollet BG, Dekel DR, Dionigi F, Deseure J, Millet P, et al. Water electrolysis: from textbook knowledge to the latest scientific strategies and industrial developments. Chem Soc Rev 2022;51:4583–762. doi:https://doi.org/10.1039/D0CS01079K.
[49] Stiller C. Design, operation and control modelling of SOFC/GT hybrid systems. Fakultet for ingeniørvitenskap og teknologi; 2006.
[50] Christiansen N, Kristensen S, Holm-Larsen H, Larsen P, Mogensen MB, Hendriksen P, et al. Status and recent advances in sofc development at haldor topsøe/risø. In: 6th European solid oxide fuel cell forum. European Fuel Cell Forum; 2004. p. 20–29.
[51] Stiller C, Thorud B, Seljebø S, Mathisen Ø, Karoliussen H, Bolland O. Finite-volume modeling and hybrid-cycle performance of planar and tubular solid oxide fuel cells. J Power Sources 2005;141:227–40. doi:https://doi.org/10.1016/j.jpowsour.2004.09.019.
[52] Liu F, Wang T, Li J, Wei T, Ye Z, Dong D, et al. Elevated-temperature bioethanol-assisted water electrolysis for efficient hydrogen production. Chem Eng J 2022;434:134699. doi:https://doi.org/10.1016/j.cej.2022.134699.
[53] Albrecht FG, König DH, Baucks N, Dietrich R-U. A standardized methodology for the techno-economic evaluation of alternative fuels – a case study. Fuel 2017;194:511–26. doi:https://doi.org/10.1016/j.fuel.2016.12.003.
[54] Maier S, Tuomi S, Kihlman J, Kurkela E, Dietrich R-U. Techno-economically-driven identification of ideal plant configurations for a new biomass-to-liquid process – a case study for central-europe. Energy Convers Manag 2021;247:114651. doi:https://doi.org/10.1016/j.enconman.2021.114651.
[55] Rahmat Y, Maier S, Moser F, Raab M, Hoffmann C, Repke J-U, et al. Techno-economic and exergy analysis of e-methanol production under fixed operating conditions in Germany. Appl Energy 2023;351:121738. doi:https://doi.org/10.1016/j.apenergy.2023.121738.
[56] Peters MS, Timmerhaus KD, et al. Plant design and economics for chemical engineers. McGraw-Hill International; 2018.
[57] Ember and Energy Institute. Carbon intensity of electricity generation, 1990 to 2023: carbon intensity is measured in grams of carbon dioxide-equivalents emitted per kilowatt-hour of electricity generated; 2024. https://ourworldindata.org/grapher/carbon-intensity-electricity?tab=chart&country=NOR.
[58] Alzate-Restrepo V, Hill JM. Effect of anodic polarization on carbon deposition on ni/ysz anodes exposed to methane. Appl Catal A Gen 2008;342:49–55. doi:https://doi.org/10.1016/j.apcata.2007.12.039.
[59] Zhou M, Liu Z, Yan X, Tan K, Tian F, Liu J. Simultaneous electrochemical reduction of carbon dioxide and partial oxidation of methane in a solid oxide cell with silver-based cathode and nickel-based anode. J Electrochem Soc 2022;169:034502. doi:https://doi.org/10.1149/1945-7111/ac554d.
[60] Xiao J, Xie Y, Liu J, Liu M. Deactivation of nickel-based anode in solid oxide fuel cells operated on carbon-containing fuels. J Power Sources 2014;268:508–16. doi:https://doi.org/10.1016/j.jpowsour.2014.06.082.
[61] Liu J, Barnett SA. Operation of anode-supported solid oxide fuel cells on methane and natural gas. Solid State Ionics 158 2003;11–16. doi:https://doi.org/10.1016/S0167-2738(02)00769-5. https://www.sciencedirect.com/science/article/pii/S0167273802007695.
[62] Kemp IC, Shiun Lim J. Pinch analysis for Energy and carbon footprint reduction: user guide to process integration for the efficient use of Energy. 3rd ed. Amsterdam: Butterworth-Heinemann; 2020. doi:https://doi.org/10.1016/C2017-0-01085-6.
[63] Jouhara H, Khordehgah N, Almahmoud S, Delpech B, Chauhan A, Tassou SA. Waste heat recovery technologies and applications. Therm Sci Eng Prog 2018;6:268–89. doi:https://doi.org/10.1016/j.tsep.2018.04.017.
[64] Mahmoudi A, Fazli M, Morad MR. A recent review of waste heat recovery by organic rankine cycle. Appl Therm Eng 2018;143:660–75. doi:https://doi.org/10.1016/j.applthermaleng.2018.07.136.
[65] Swanson RM, Platon A, Satrio JA, Brown RC. Techno-economic analysis of biomass-to-liquids production based on gasification. Fuel 2010;89:S11–19. doi:https://doi.org/10.1016/j.fuel.2010.07.027.
[66] Union E. Electricity prices for non-household consumers - bi-annual data (from 2007 onwards); 2024. Retrieved 10 Oct. 2024, from https://ec.europa.eu/eurostat/databrowser/view/nrg_pc_203/default/table?lang=en.
[67] Chen C, Rubin ES. CO_2 control technology effects on IGCC plant performance and cost. Energy Policy 2009;37:915–24. doi:https://doi.org/10.1016/j.enpol.2008.09.093.
[68] C. A. R. M. E. N. e.V. Marktpreise hackschnitzel; 2023. Präsentwicklung bei Waldhackschnitzeln. Retrieved 12 Apr. 2023, from https://www.carmen-ev.de/service/marktueberblick/marktpreise-energieholz/marktpreise-hackschnitzel/.
[69] OECD. Pricing greenhouse gas emissions: key findings; 2024. Retrieved 24 Oct. 2024, from https://www.oecd.org/content/dam/oecd/en/topics/policy-sub-issues/carbon-pricing-and-energy-taxes/carbon-pricing-norway.pdf.
[70] Union E. Gas prices for non-household consumers - bi-annual data (from 2007 onwards); 2023. Retrieved 5 Jun. 2023, from https://ec.europa.eu/eurostat/databrowser/view/nrg_pc_203/default/table?lang=en.
[71] Kirschner MJ, Alekseev A, Dowy S, Grahl M, Jansson L, Keil P, et al. Oxygen. In: Ullmann's encyclopedia Of industrial chemistry; 2000. p. 1–32.
[72] Pratschner S, Hammerschmid M, Müller S, Winter F. Off-grid vs. grid-based: techno-economic assessment of a power-to-liquid plant combining solid-oxide electrolysis and Fischer-Tropsch synthesis. Chem. Eng. J. 2024;481:148413. doi:https://doi.org/10.1016/j.cej.2023.148413.
[73] Herz G, Rix C, Jacobasch E, Müller N, Reichelt E, Jahn M, et al. Economic assessment of power-to-liquid processes – influence of electrolysis technology and operating conditions. Appl Energy 2021;292:116655. doi:https://doi.org/10.1016/j.apenergy.2021.116655.
[74] Markowitsch C, Lehner M, Maly M. Evaluation of process structures and reactor technologies of an integrated power-to-liquid plant at a cement factory. J CO2 Util 2023;70:102449. doi:https://doi.org/10.1016/j.jcou.2023.102449.
[75] Putta KR, Pandey U, Gavrilovic L, Rout KR, Rytter E, Blekkan EA, et al. Optimal renewable energy distribution between gasifier and electrolyzer for syngas generation in a power and biomass-to-liquid fuel process. Front Energy Res 2022;9. doi:https://doi.org/10.3389/fenrg.2021.758149.
[76] Jensen SH, Sun X, Ebbesen SD, Chen M. Pressurized operation of a planar solid oxide cell stack. Fuel Cells 2016;16:205–18. doi:https://doi.org/10.1002/fuce.201500180.